DMI
Ministry of Transport and Energy

Scientific Report 07-01

Sea clutter removal using radar elevation dependent second order texture parameters

Rashpal S. Gill

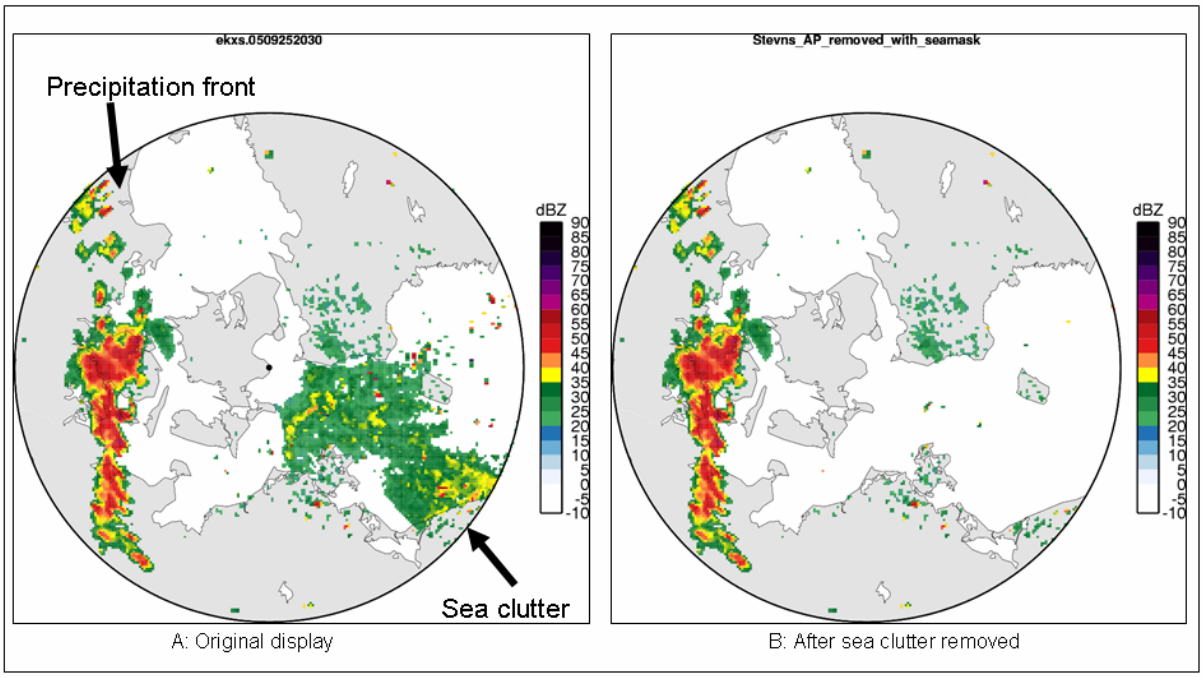

A: Original display

B: After sea clutter removed

Copenhagen 2007

Colophon

Serial title:
Scientific Report 07-01

Title:
Sea clutter removal using radar elevation dependent second order texture parameters

Subtitle:

Author(s): Rashpal S. Gill

Other contributors:

Responsible institution:
Danish Meteorological Institute

Language:
English

Keywords:
Sea clutter removal. Second order texture parameters.

Url:
www.dmi.dk/dmi/sr07-01

Digital ISBN:
978-87-7478-544-6

ISSN:
1399-1949

Version:

Website:
www.dmi.dk

Content:

Abstract

One of the main characteristic of clutter is that it is confined to low elevation angles, typically ≤ 1.5°- 2.0º. To make optimal use of this information new elevation angle dependent second order texture parameters are proposed. The formulation is based on the Elevation Dependent Co-occurence Matrix (EDCM) which is a measure of the number of occurrences of pixels at elevation angles I and J having reflectivity values > Z_{min}. One of the striking features of the model is that the contribution to texture made by low reflectivity values, $Z \leq Z_{min}$, are also included. From the EDCM a number of second order texture parameters can be defined and these are used to determine their effectiveness at discriminating between clutter and precipitation. In the evaluation so far the texture parameters entropy, inertia, uniformity and inverse difference moment have been used. It was found that the parameter inertia is exceptionally effective at discriminating between clutter and precipitation. However, a general clutter removal model that does not 'accidentally' remove precipitation pixels is difficult. Thus to minimize the 'accidental' removal of precipitation pixels, it is proposed to implement a land and/or sea clutter removal algorithm for the individual radars, making use of the additional information that is specific to the radar. The latter can, for example, be restricting the application of the clutter removal model to specific geographical 'hot spots' where clutter is frequently observed by the radar and taking into account other relevant local information such as its seasonal dependence. One such model, to remove the sea clutter, has been developed for the Danish Meteorological Institute's (DMI) radar at Stevns on the island Sjælland (55.326°N, 12.449°E). The evaluation of the model undertaken so far looks encouraging. Further tests of the model, during routine operations, are in progress. In this article the details of the method is described and some results of the evaluation are presented.

Resumé

Et af de vigtigste karakteristika af clutter er at det er begrænset til lave elevationsvinkler. Dette udnyttes her til at lave en model til adskillelse af clutter og nedbør baseret på nye strukturparametre der er afhængige af elevationsvinklen.

1. Introduction

One of the main problems of observing precipitation with weather radars is that they tend to be contaminated by non-precipitation echoes. These so-called false echoes can be split into three general categories: (1) false echoes that occur because of the radar signals are backscattered from non-hydrometeors in the atmosphere, such as flying aircrafts, birds, insects etc., (2) signals received from external radio emitters including the Sun etc., and (3) those false alarms that occur naturally due to the abnormal propagation of the radar signals. Many of these false alarms have been known since the early days when radars were first employed for weather observations and the meteorological conditions that give rise to them are well described in the literature (Booker, 1946, Batten, 1973, Skolnik, 1980, Doviak and Zrnic, 1993, Meischner, 2004).

This report is concerned with the false alarms that falls in the last category, namely due to anomalous propagation effects, commonly termed anaprop or AP. To understand what anaprop is and how it occurs, one has to consider the refractive index variations of the atmosphere. Briefly, according to the definitions given in Sklonik (1980) anaprop occurs when the refractive index gradient, dn/dh, lies outside the 'normal refraction' range from 0 to $-0.787*10^{-7}$ m^{-1}. The commonly used standard 4/3*R atmospheric model results when the refractive index decreases uniformly with altitude at the rate of $-3.9*10^{-8}$ m^{-1}. The terms that are commonly used to describe types of anaprop are sub-refraction, super-refraction, and ducting. Of these three it is the latter two that are most serious as far as false alarms are concerned as the radar waves are abnormally bent towards the earth's surface resulting in the worse case backscatter signals from the ground at ranges far way from the radar site. These false echoes from the earth's surface can be split into two classes: (i) land clutter, and (ii) sea clutter. Land clutter is generally characterised by near zero doppler velocities and because of this doppler radars have been very successful in removing them or at least minimizing the effect of this form of false echoes (Doviak and Zrnic, 1993, Meischner, 2004). Removal of sea clutter in the radar returns, on the other hand, is much more difficult as the radar returns from the sea can be of comparable strength (~ 15 dBZ - 20 dBZ is not uncommon) and have similar doppler velocities to radar returns from precipitation regions. In recent years dual polarisation radars are increasingly becoming popular because of their potential to discriminate between different types of precipitation e.g., snow, light and heavy rain, hail etc. (Bringi and Chandrasekar, 2001, Ryzhkov, 2006). Further, from the point of view of this report, these types of radars also appear to be very promising at discriminating between false echoes from land/sea and actual precipitation (Sugier and Tabary, 2006). However, the dual polarisation weather radar technology is not the subject of this report. It is concerned mainly at discriminating between sea clutter and precipitation signals in single polarisation doppler weather radars, as these radars are still the primary 'work horses' at national weather services.

A number of techniques have been reported in the open literature to remove sea clutter signals in the radar data. Some of these more advanced techniques make use of neural network and fuzzy logic classifiers using local statistical parameters such as mean, median, standard deviations, and texture features such as homogeneity (Lakshmanan et. al., 2003, Kissinger et. al., 2003). Other features such as SPIN, SIGN, thresholds on the vertical reflectivity, vertical gradients, maximum elevation scans at which reflectivity are observed (ECHOtop) have also been used (Steiner and Smith, 2002, Kissinger, 2003). In the decision tree algorithm implemented by Steiner and Smith (2002), for example, the following steps are applied sequentially: (i) remove all pixels values < 5 dBZ, (ii) now remove all pixels that have reflectivity only in the lowest elevation scan (ECHOtop = lowest scan angle), (iii) of the remaining pixels, if their SPIN, defined as the number of reflectivity fluctuations > 2 dBZ in a window of size 11*21 pixels, < SPINthreshold, they are also removed, (iv) of the remaining pixels, if their vertical gradients is > 10 dBZ/degree, they are also considered

to be false alarms. The pixels that remain after steps (i) – (iv) are considered to be true precipitation.

Less advanced methods oriented towards routine operations have also been developed; based exclusively on the vertical variability of the reflectivity above a given point (Alberoni et. al., 2001). In the simpler of these methods developed at the Servizio Meteorological Regionale (SMR) of Italy, the differences between the radar reflectivity V_1 and V_2 at the elevation angles 0.5º and 1.4º, respectively are computed. Ananprop is declared when this difference $(V_1 - V_2) > T_1$ or when this difference > 0 and $V_2 < T_2$, where T_1 and T_2 are thresholds. In another method operational at the Swedish Meteorological and Hydrological Institute (SMHI), statistical parameter Mean Square Deviation (MSD) which is defined by $\frac{1}{n}\sum d_i^2$, where $d_i = V_i - V_{i+1}$, the difference between the radar reflectivity at elevation angles, i and i+1 are used. n is the number of elevation scans used in the analysis (typically 7 from 0.5º to 1.2º). According to the investigations at SMHI, normal precipitation is expected to occur for $0 \leq$ MSD ≤ 16 dBZ^2 and the vertical reflectivity profile must be even and unbroken, anaprop over land contain uneven and/or broken reflectivity profiles and MSD > 16 dBZ^2 or < 0 dBZ^2. Sea clutter is characterised by broken reflectivity profiles and MSD < 0 dBZ^2. Further parameters FUP (Frequency of Unbroken Profiles) and FAMSD (Frequency of Accepted MSD) defined for a (n x n) pixels window are proposed, and if a pixel over land has FAMSD < FAMSDthreshold, then it is classified as land clutter. Similarly if FUP < FUPthreshold for a pixel over the sea, then it is classified as sea clutter.

The methods outlined above to remove ananprop are predominately based on the radar reflectivity data, Z, and occasionally V (doppler velocity) and W (doppler spectrum width). However, in addition to above methods, alternative techniques have also been proposed. One well known method make use of the pulse to pulse raw radar signals to discriminate between clutter and precipitation pixels (Wessel and Beekhuis, 1994). Other methods that are increasing becoming popular are based on using satellite and surface data, including derived products, to discriminate between precipitation and anaprop regions (Michelson and Sunhede, 2004, Lakshmanan and Valente, 2004, Bøvith et al., 2006).

A technique that has a special relevance to the method outlined in this report is based on the second order texture parameters based on the Grey Level Co-occurrence Matrix (GLCM) (Haralick (1973)). GLCM is a count of the number of occurrences of two neighbouring pixels, at different locations within a square window of size W*W which have grey values i and j. A number of texture parameters can be computed from the GLCM, with entropy, inertia, energy, local homogeneity being the most popular, and these have been used extensively in other branches of remote sensing for image classification (e.g., Gill, 2001). In the context of weather radars, it was found that the texture parameters energy and local homogeneity, out of total of 9 odd parameters, applied to the pseudo CAPPI data, were the most effective at discriminating between precipitation and false echoes (Haddad et. al., 2004).

Many of the techniques outlined above to remove anaprop are based predominately on thresholds applied to Z, gradients of Z and/or differences of Z at different elevation scans, or parameter such as FUP measuring the frequency of vertical unbroken profiles. The reason why reflectivity values at different elevation scans are so important for anaprop recognition is that it has long been observed that clutter signals have little vertical extent and that they tend to be confined to low elevation angles, typically ≤1.5°- 2.0º. Thus one way to improve anaprop recognition in weather radar data is to devise more effective altitude dependent texture parameters. One such method is proposed and is the subject of this report. In particular, a new matrix by analogy with the GCLM is proposed. However, unlike the GLCM which is a measure of the number of occurrences of two neighbouring pixels, at two different locations with grey values i and j, the current matrix is a measure of the

number of occurrences of pixels at elevation angles I and J having reflectivity values > Z_{min}. By analogy with the GLCM a number of texture parameters can be defined and these are used to determine their effectiveness at distinguishing between sea clutter and precipitation.

In the next chapter the detail of the proposed method is given. Chapters 3 and 4 deals with sensitivity studies using simulated and real radar data, respectively. Chapter 5 deals with the analysis of clutter suppression using texture parameters. In chapter 6 sea clutter removal model is proposed. Finally in chapter 7 summary of the results obtained so far are given.

2. Second order elevation angle dependent texture parameters

As mentioned in the introduction one of the main feature that distinguish anomalous propagation signals from real precipitation is that the former have little vertical extend i.e., it tends to be confined to low elevations, typically $\leq 1.5°$- 2.0º. This can be seen in fig. 1 which shows reflectivity values obtained at elevation scan angles 0.5°, 0.7°, 1.0° and 1.5° (sub-figures A to D, respectively). The data were obtained using the Danish Meteorological Institute's (DMI) weather radar situated on the main island of Sjælland at Stevns; about 50 meters from the Baltic Sea coast (55.326°N, 12.449°E). The images show a precipitation front approaching from south west (left side of each image) and land and sea clutter regions in the centre and south east regions.

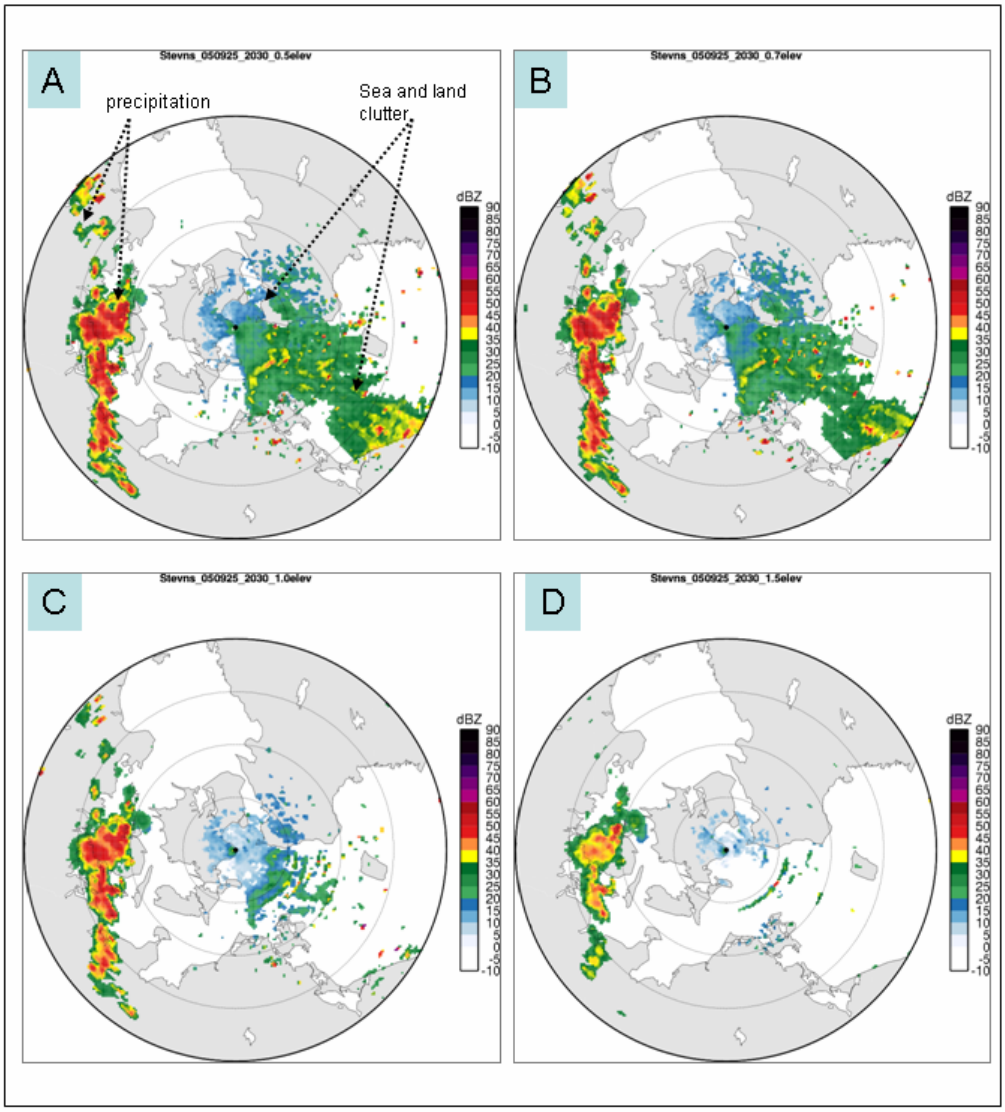

Fig. 1 The radar reflectivity, Z (dBZ), measured at different elevation scan angles 0.5, 0.7, 1.0 and 1.5 (clockwise figures A to D) respectively, at the DMI radar situated at Stevns from 25th Sept. 2005 20:30 UTC. The images show a precipitation front on the left and a land and sea clutter from the centre and right of the images. The distance to the outer most circles is 240 km from the centre (position of the radar) and each inner concentric circle are at a radius of 60 km.

Further, by taking a vertical slice through the sea clutter and precipitation regions shown in fig. 1, one can see the distribution of actual reflectivity values in the individual range gates in these two areas. This can be seen in fig. 2 which shows the typical rays in the precipitation and clutter regions. From this figure it is clear that there are fewer empty range gates in the precipitation region than in the clutter area, as observed earlier (Alberoni et. al., (2001)). Further it appears that the precipitation reflectivity values are often higher than those in the clutter regions, however, this is not always true, especially in moderate precipitation weather conditions.

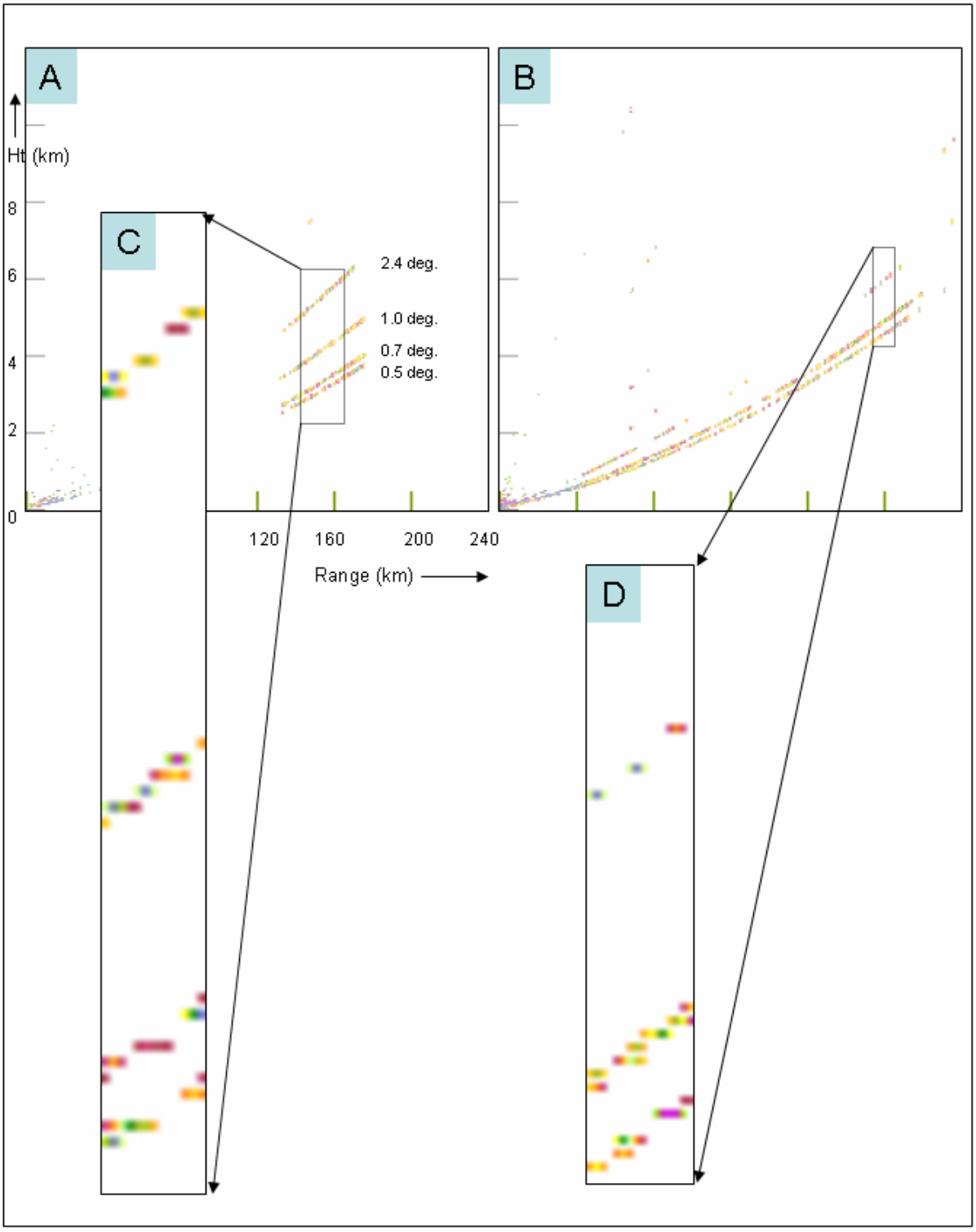

Fig. 2 Typical vertical slices of reflectivity Z (grey levels) through the precipitation front (figs. A and C above) and the sea clutter region (figs. B and D above)

To discriminate between precipitation and clutter, it is clear that 'capturing' the information about the magnitude and the distribution of the reflectivity values in the individual range gates in the volume elevation scan angles data would be significant. One method to do this, which is proposed in this report, is to 'construct' texture parameter(s) that are dependent on the radar elevation scan angles.

In the section 2.1, the Elevation angle Dependent Co-occurrence Matrix (EDCM) which forms the basis of the proposed texture parameter(s) is derived. Section 2.2 describes the definition of the EDCM texture parameters.

2.1 Elevation Angle Dependent Co-occurrence matrix

As mentioned in the introduction GLCM is a count of the number of occurrences of two neighbouring pixels, at different locations within a square window of size W*W which have grey values i and j (Haralick et. al., 1973). GLCM is generally evaluated along directions 0º, 90º, 45º and 135º. The texture parameters that are computed using the GLCM are computationally very demanding as it involves a double summation over all grey values (255 for an 8-bit data) for each pixel within a window of size W*W. What is generally done is to reduce the grey level resolution of the original data from 8-bit to an acceptable level. In the context of the weather radar data, to classify pseudo CAPPI products, using GLCM method 52 grey levels have been used (Haddad et. al., 2004)).

It is clear from the brief introduction on the GLCM that its elements do not contain any information on the vertical extent of the radar reflectivity values. However, by analogy with the GLCM, a simple matrix can be constructed that is dependent on the radar elevation scan angles. This is outlined in the section 2.1.1 below.

2.1.1 Derivation of the EDCM matrix

This section is essentially split into two parts; in the first part the main aspects of the EDCM are introduced and in second part the texture parameters that can be defined from it are given including their physical interpretations.

Consider a window, W, of size ($W_R \times W_A \times W_\phi$) where W_R, W_A and W_ϕ are its dimension in the radial, azimuth and elevation direction, respectively. Then the non-normalised elements of the EDCM, denoted by N_{ij}, for the ground pixel situated at point p, at the centre of the 2 dimensional window of size ($W_R \times W_A$), represent the number of occurrences of radar gates, for a fixed single value of azimuth angle, A_k, at locations (R_1, ϕ_i) and (R_2, ϕ_j), having a pair of reflectivity values $> Z_{\min}$. In the special case of i=j, there is no pair of values as it then refers to the single reflectivity value at elevation scan angle $\phi_{i=j}$. Further, fractional occurrences are also allowed. This is required to model the special case when pair of reflectivity values $(Z_i, Z_j) < Z_{\min}$. In particular, if

(Z_i, Z_j) lies in the range $Z_{th} < (Z_i, Z_j) \le Z_{\min}$ where Z_{th} is the minimum threshold value (=0 dBZ, for example), then elements of the EDCM, denoted by N_{ij}, are assumed to be given by the following simple linear expression

$$N_{ij} = \frac{MIN(Z_i, Z_j)}{(Z_{\min} - Z_{th})} \qquad (1)$$

where MIN denotes the minimum of the two reflectivity values.

A sketch of the proposed window is shown in fig. 3. The two neighbouring pixels can in principle be separated by a displacement vector, **D,** of magnitude D and direction θ (Shokr, 1991).

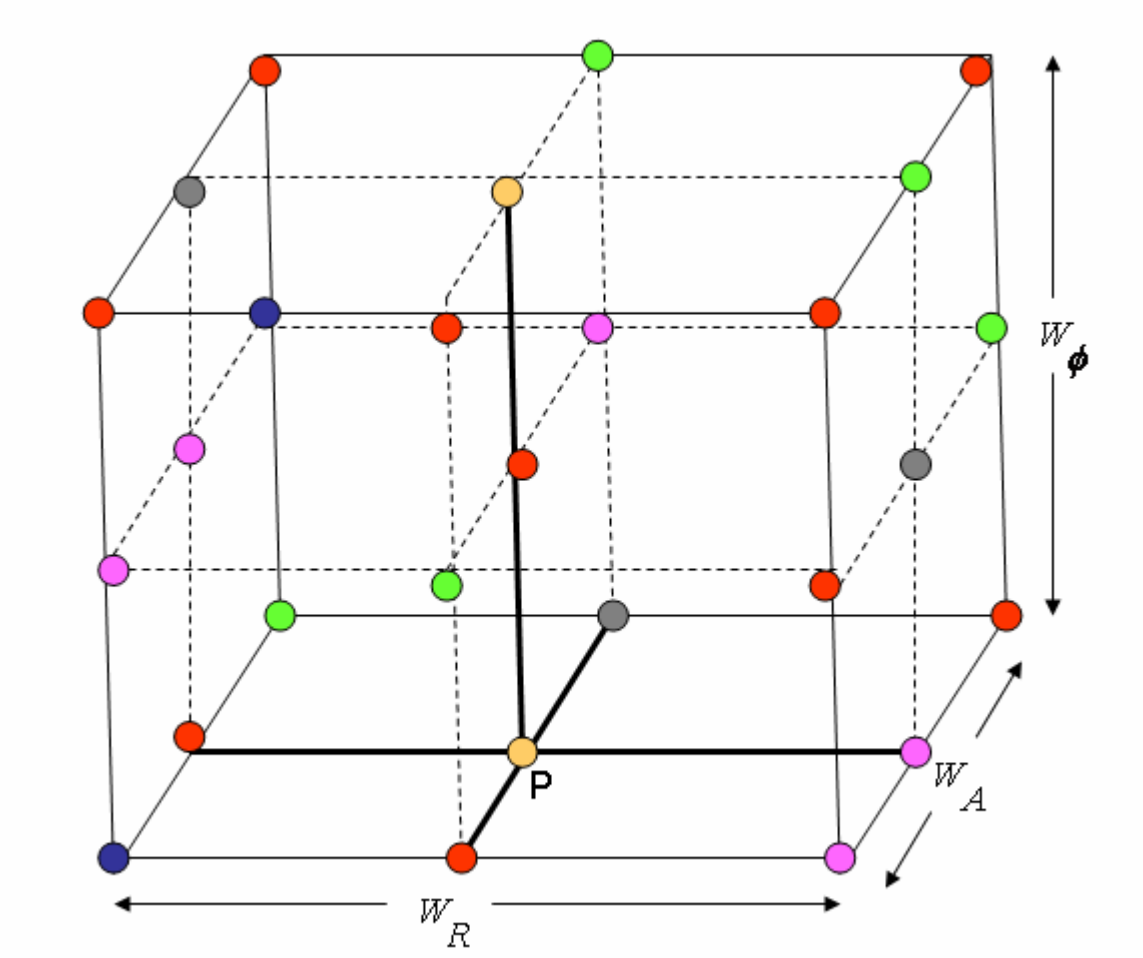

Fig. 3 A sketch of the 3 dimensional window of size ($W_R \times W_A \times W_\phi$) used to compute the elements of the EDCM N_{ij} for the ground pixel, P situated at the centre of the 2 dimensional window of size ($W_R \times W_A$). The colour spots are used to indicate the different reflectivity values at different range gates.

N_{ij} is a square symmetric matrix of size ($W_\phi \times W_\phi$) i.e. the number of elevations scans angles used. By analogy with the GCLM, for each value of the azimuth angle, A_k, the elements of N_{ij} can

be computed in the 4 discrete directions; (i) (0° & 180°), (ii) (45° & 225°), (iii) (90° & 270°) and (iv) (135° & 315°). Computation of N_{ij} in the horizontal direction (0° & 180°) has perhaps little relevance for sea clutter discrimination using vertical distribution of reflectivity values, and is given here for completion. The geometrical configuration is illustrated in fig. 4 below for a window consisting of 3 range gates and 3 elevation scan angles i.e., $(W_R \times W_\phi)$ = (3 X 3). **D** is set to 1.

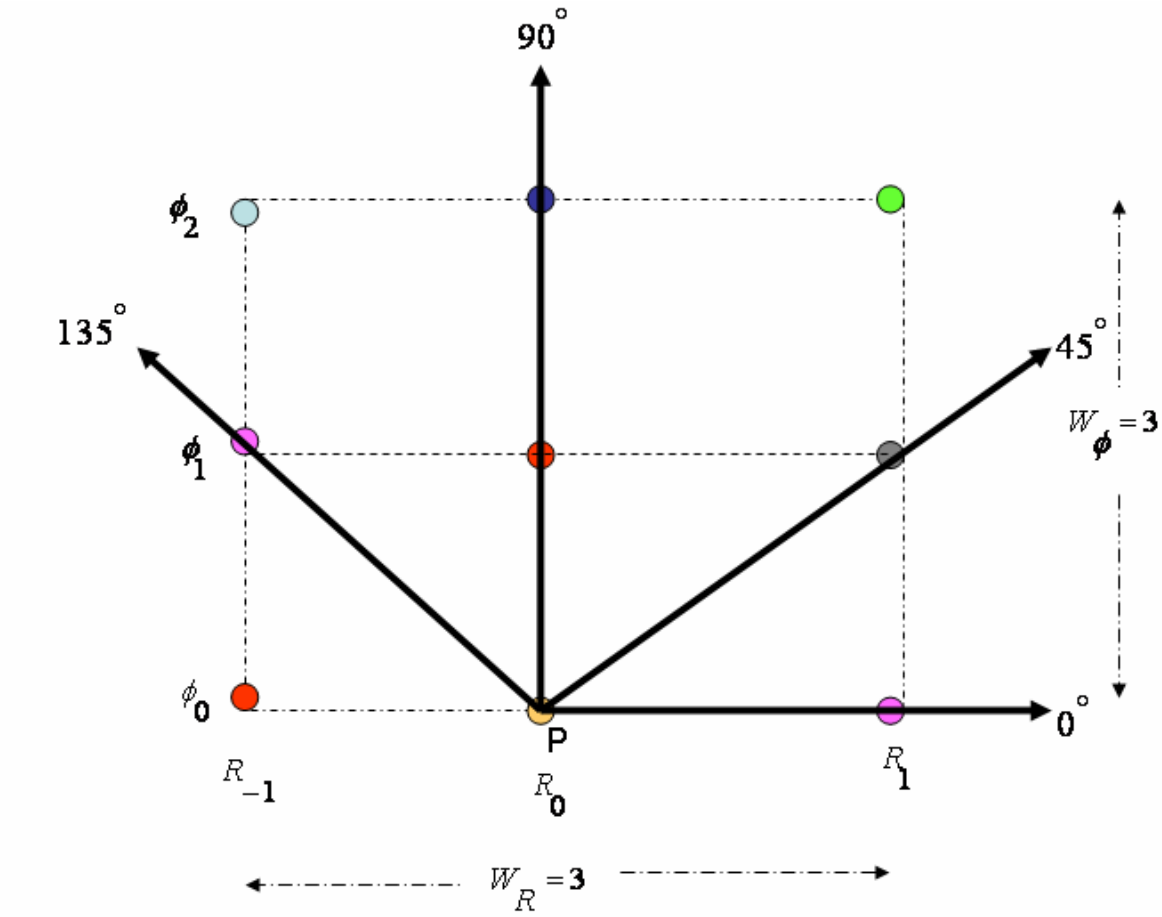

Fig. 4 A sketch of the 2 dimensional window $(W_R \times W_\phi)$ = (3 X 3) i.e., consisting of 3 range gates and 3 elevation scan angles, for $W_A = 1$ showing computational directions 0°, 45°, 90° and 135°.

The normalised components of the N_{ij}, in the pair of 4 discrete directions are given by the following expressions.

(i) Direction (0°, 180°): $N_{ij} = \dfrac{N_{ij}}{(W_A \times W_R^2)}$, all elements with $i \neq j$ are 0.

(ii) Direction (90°, 270°): $N_{ij} = \dfrac{N_{ij}}{(W_A \times W_R)}$

(iii) Directions (45°, 225°) and (135°, 315°):

$$N_{ij} = \frac{1}{W_A} \times \left\{ \frac{N_{ii}}{W_R}, \quad \frac{N_{i\pm m,i}}{(W_R - m)}, \quad \frac{N_{i,i\pm m}}{(W_R - m)} \right\}, \text{ for m=1,2, } \ldots W_\phi - 1.$$

2.2 Elevation angle Dependent Texture parameters

By analogy with the GLCM, a number of texture parameters can be defined for the EDCM (Haralick, 1973). From this list four were selected for sea clutter precipitation discrimination. These are: Entropy (ENT), Inverse Difference Moment (IDM) also called Local Homogeneity, Inertia (INER) also called Contrast, Uniformity (UNIF) also called Energy. They are given by the following expressions:

$$ENT = \sum_j \sum_i - N_{ij} \log_e (N_{ij})$$

$$IDM = \sum_j \sum_i \frac{1}{1 + (i - j)^2} N_{ij} \qquad (2)$$

$$INER = \sum_j \sum_i (i - j)^2 N_{ij}$$

$$UNIF = \sum_j \sum_i \left[N_{ij} \right]^2$$

As regards to what each of the texture parameters measure, very briefly, entropy, as in statistics, is a measure of order/disorder in a particular direction in the 3 [D] window shown in fig. 3. For example, in the vertical direction, if all the reflectivity values are the same then entropy values will be zero. Similarly, inertia which is sometime also called contrast is largest for EDCM elements that are furthest apart from one another and is zero for the diagonal elements of N_{ij}. For example, inertia computed in the vertical direction will be largest if there is a pair of reflectivity values $\geq Z_{\min}$ in the lowest and the highest elevations, e.g., 0.5º and 1.5º, respectively, because of the factor $(i - j)^2$. IDM is a measure of local homogeneity and is largest for N_{ij} elements that lie on or near the diagonal. Finally, uniformity is a measure of so-called energy and will be largest if all the elements N_{ij} are full. However, it should be noted from the formulation presented above, the maximum value that the normalised element of the matrix N_{ij} can take is 1. In general case, the elements of $N_{ij} \leq 1$.

In chapter 3 simulated examples are given to illustrate the sensitivity of the N_{ij} and hence the texture parameters to possible distribution of the reflectivity values in the 4 directions given above. In all the examples, $W_A = 1$, $(W_R \times W_\phi)$ = (3 X 4) i.e., window consisting of 3 range gates and 4 elevation scan angles with Z_{th}=0 dBZ and $Z_{\min}$=10 dBZ.

3. Texture parameter's sensitivity estimates using simulated data

In this chapter the texture parameters defined above are computed in the 4 discrete directions; (i) (0° & 180°), (ii) (45° & 225°), (iii) (90° & 270°) and (iv) (135° & 315°) for different cases of simulated data to estimate their probable sensitivities.

3.1 Simulated case study 1

Consider a window with the reflectivity values as given in fig. 5. Note that in this case there are no empty gates and further that all reflectivity values, Z_i are $\geq Z_{\min}$. This could be an example of possible moderate precipitation.

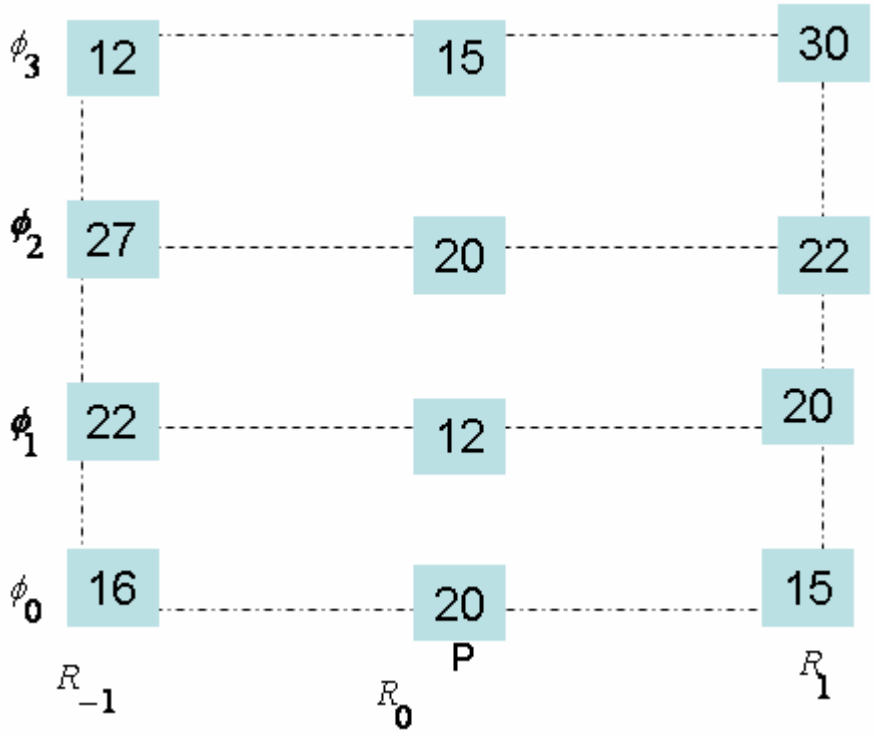

Fig. 5 Simulated example indicating the reflectivity values for a window ($W_R \times W_\phi$) = (3 X 4)

In this case normalised elements of N_{ij} in the (0°, 180°) are given in table 1 below.

1	0	0	*0*
0	1	0	*0*
0	0	1	*0*
0	0	0	1

Table 1. Normalised elements of the EDCM matrix N_{ij} in the horizontal direction (0°, 180°).

Similarly in the directions (90°, 270°), (45°, 225°) and (135°, 315°) N_{ij} normalised elements are all equal and are given in table 2.

1	1	1	1
1	1	1	1
1	1	1	1
1	1	1	1

Table 2. Normalised elements of the EDCM matrix N_{ij} in the directions (90°, 270°), (45°, 225°) and (135°, 315°).

The numerical values of the 4 texture parameters defined in (2), in the 4 directions discussed above, are given in table 3.

	ENT (for N_{ij} >0)	IDM	UNIF	INER
(0°, 180°)	0.0	4.0	4.0	0.0
(90°, 270°)	0.0	8.0	16.0	40.0
(45°, 225°)	0.0	7.8	14.0	22.0
(135°, 315°)	0.0	7.8	14.0	22.0

Table 3. The values of the 4 texture parameters ENT, IDM, UNIF and INER, in the 4 directions (90°, 270°), (45°, 225°) and (135°, 315°), for the simulated reflectivity values depicted in fig. 5.

Note that ENT is partly undefined for those elements of N_{ij} =0 as loge (N_{ij} =0) is infinity. Therefore the ENT values given in table 3 are defined for N_{ij} >0. Further, note the dynamic range of the texture parameters. As all the reflectivity values in the test window, fig. 5, are $\geq Z_{\min}$, the table 3 gives the maximum expected dynamic ranges. These ranges are largest for inertia in the vertical directions (90°, 270°). Likewise, the texture parameters have the least dynamical ranges in the horizontal directions **(**0°, 180°).

3.2 Simulated case study 2

Consider a window with the reflectivity values as given in fig. 6. Note that in this case some gates have reflectivity values equal to 0 ($=Z_{th}$) while the remaining all have values $\geq Z_{\min}$.

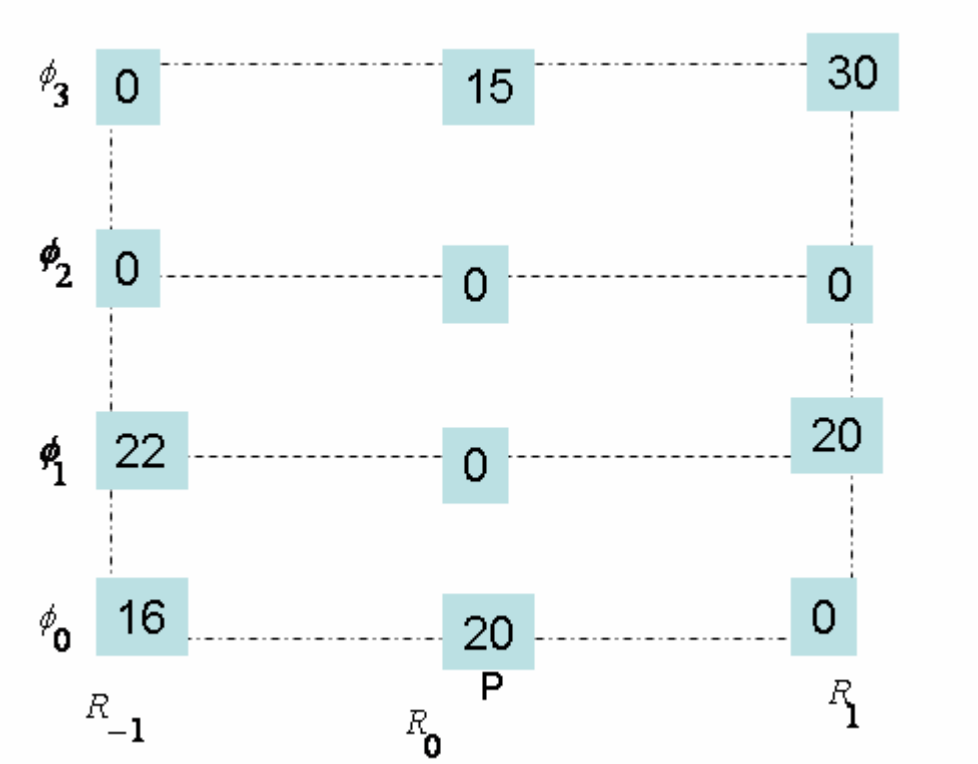

Fig. 6 Simulated example indicating the reflectivity values for a window ($W_R \times W_\phi$) = (3 X 4).

In this case normalised elements of N_{ij} in the (0°, 180°) are given in table 4 below.

4/9	0	0	0
0	4/9	0	0
0	0	0	0
0	0	0	4/9

Table 4. Normalised elements of the EDCM matrix N_{ij} in the horizontal direction (0°, 180°) for the simulated reflectivity data in fig. 6.

Similarly in the directions (90°, 270°) they are given in table 5.

2/3	1/3	0	1/3
1/3	2/3	0	1/3
0	0	0	0
1/3	1/3	0	2/3

Table 5. Normalised elements of the EDCM matrix N_{ij} in the horizontal direction (90°, 270°) for the simulated reflectivity data in fig. 6.

In the directions (45°, 225°) they are given in table 6.

2/3	1/2	0	0
1/2	2/3	0	1
0	0	0	0
0	1	0	2/3

Table 6. Normalised elements of the EDCM matrix N_{ij} in the horizontal direction (45°, 225°) for the simulated reflectivity data in fig. 6.

Finally, in the directions (135°, 315°) they are given in table 7.

2/3	1/2	0	0
1/2	2/3	0	0
0	0	0	0
0	0	0	2/3

Table 7. Normalised elements of the EDCM matrix N_{ij} in the horizontal direction (135°, 315°) for the simulated reflectivity data in fig. 6.

The numerical values of the 4 texture parameters defined in (2), in the 4 directions mentioned above, are given in table 8.

	ENT (for N_{ij} >0)	**IDM**	**UNIF**	**INER**
(0°, 180°)	1.081	1.333	0.593	0.000
(90°, 270°)	3.001	2.533	2.000	9.333
(45°, 225°)	1.504	2.900	3.833	9.000
(135°, 315°)	1.504	2.500	1.833	1.00

Table 8. The values of the 4 texture parameters ENT, IDM, UNIF and INER, in the 4 directions (90°, 270°), (45°, 225°) and (135°, 315°), for the simulated reflectivity values depicted in fig. 6.

The dynamical ranges of IDM and entropy are only 1.333 – 2.900 and 1.081 – 3.001, respectively in the 4 computational directions. Similarly UNIF is slightly better with the values lying in the range 0.593 – 3.883. Inertia values varies between 0.000 – 9.333.

3.3 Simulated case study 3

In this case consider the reflectivity values as depicted in fig. 7. Note that in this case some of the reflectivity values Z_i are $\leq Z_{\min}$ and $\leq Z_{th}$ and for these pixels equ. (1) is used to compute the elements of N_{ij}. This example could be representative of possible land/sea clutter.

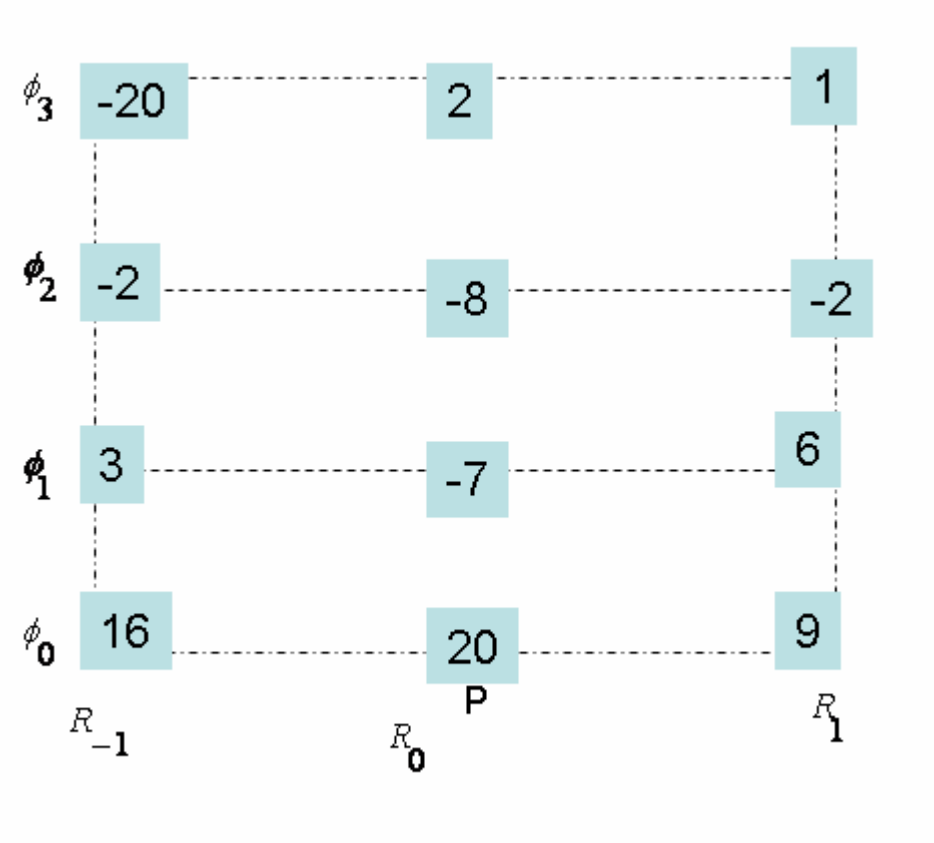

Fig. 7 Simulated example indicating the reflectivity values for a window ($W_R \times W_\phi$) = (3 X 4).

In this case normalised elements of N_{ij} in the (0°, 180°) are given in table 9 below.

8.5/9.0	0	0	0
0	1.5/9.0	0	0
0	0	0	0
0	0	0	0.5/9.0

Table 9. Normalised elements of the EDCM matrix N_{ij} in the horizontal direction (0°, 180°) for the simulated reflectivity data in fig. 7.

Similarly in the directions (90°, 270°) they are given in table 10.

2.9/3.0	0.9/3.0	0	0.3/3.0
0.9/3.0	0.9/3.0	0	0.1/3.0
0	0	0	0
0.3/3.0	0.1/3.0	0	0.3/3.0

Table 10. Normalised elements of the EDCM matrix N_{ij} in the horizontal direction (90°, 270°) for the simulated reflectivity data in fig. 7.

In the directions (45°, 225°) they are given in table 11.

2.9/3.0	0.6/2.0	0	0
0.6/2.0	0.9/3.0	0	0.1
0	0	0	0
0	0.1	0	0.3/3.0

Table 11. Normalised elements of the EDCM matrix N_{ij} in the horizontal direction (45°, 225°) for the simulated reflectivity data in fig. 7.

Finally, in the directions (135°, 315°) they are given in table 12.

2.9/3.0	0.3/2.0	0	0
0.3/2.0	0.9/3.0	0	0
0	0	0	0
0	0	0	0.3/3.0

Table 12. Normalised elements of the EDCM matrix N_{ij} in the horizontal direction (135°, 315°) for the simulated reflectivity data in fig. 7.

The numerical values of the 4 texture parameters defined in (2), in the 4 directions mentioned above, are given in table 13.

	ENT (for N_{ij} >0)	IDM	UNIF	INER
(0°, 180°)	0.513	1.667	0.923	0.000
(90°, 270°)	2.034	1.700	1.237	2.667
(45°, 225°)	1.807	1.706	1.234	1.400
(135°, 315°)	1.193	1.517	1.079	0.300

Table 13. The values of the 4 texture parameters ENT, IDM, UNIF and INER, in the 4 directions (90°, 270°), (45°, 225°) and (135°, 315°), for the simulated reflectivity values depicted in fig. 7.

In this case the dynamical ranges of IDM and UNIF are only 1.517 – 1.706 and 0.923 – 1.237, respectively in the 4 computational directions. Similarly entropy is slightly better with the values lying in the range 0.513 – 2.034. Inertia values varies between 0.000 – 2.667.

3.4 Simulated case study 4

Final example is given in fig. 8. In this case the reflectivity values for the top 2 elevations are very low ($\leq Z_{th}$) and all but one of range gates for the remaining elevations have reflectivity values $\leq Z_{\min}$. This example could be representative of weak low lying land/sea clutter.

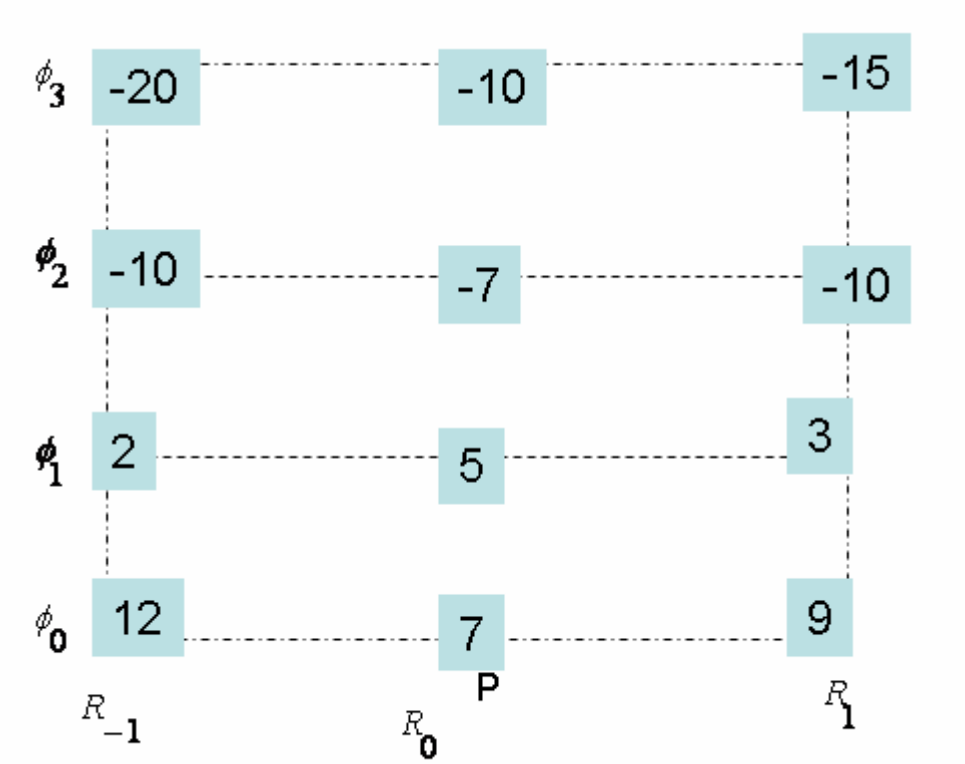

Fig. 8 Simulated example indicating the reflectivity values for a window ($W_R \times W_\phi$) = (3 X 4).

In this case normalised elements of N_{ij} in the (0°, 180°) are given in table 14 below.

7.2/9.0	0	0	0
0	2.4/9.0	0	0
0	0	0	0
0	0	0	0

Table 14. Normalised elements of the EDCM matrix N_{ij} in the horizontal direction (0°, 180°) for the simulated reflectivity data in fig. 8.

Similarly in the directions (90°, 270°) they are given in table 15.

2.6/3.0	1.0/3.0	0	0
1.0/3.0	1.0/3.0	0	0
0	0	0	0
0	0	0	0

Table 15. Normalised elements of the EDCM matrix N_{ij} in the horizontal direction (90°, 270°) for the simulated reflectivity data in fig. 8.

In the directions (45°, 225°) they are given in table 16.

2.6/3.0	0.8/2.0	0	0
0.8/2.0	1.0/3.0	0	0
0	0	0	0
0	0	0	0

Table 16. Normalised elements of the EDCM matrix N_{ij} in the horizontal direction (45°, 225°) for the simulated reflectivity data in fig. 8.

Finally, in the directions (135°, 315°) they are given in table 17.

2.6/3.0	0.7/2.0	0	0
0.7/2.0	1.0/3.0	0	0
0	0	0	0
0	0	0	0

Table 17. Normalised elements of the EDCM matrix N_{ij} in the horizontal direction (135°, 315°) for the simulated reflectivity data in fig. 8.

The numerical values of the 4 texture parameters defined in (2), in the 4 directions mentioned above, are given in table 18.

	ENT (for N_{ij} >0)	IDM	UNIF	INER
(0°, 180°)	0.531	1.067	0.711	0.000
(90°, 270°)	1.223	1.533	1.084	0.667
(45°, 225°)	1.223	1.600	1.182	0.800
(135°, 315°)	1.225	1.550	1.107	0.700

Table 18. The values of the 4 texture parameters ENT, IDM, UNIF and INER, in the 4 directions (90°, 270°), (45°, 225°) and (135°, 315°), for the simulated reflectivity values depicted in fig. 8.

Comparing the values of the texture parameters given in tables 3 and 18 representing the two extreme cases, one representing possible precipitation and the other low lying clutter, it can be seen that inertia has the largest dynamical difference between the 2 cases, especially in the vertical directions, (90°, 270°) (INER = 0.667 to 40). This is followed by inertia values in the diagonal directions (INER= 0.8 to 22). Purely from the dynamical ranges of the texture parameters, uniformity is expected to the next best discriminator, followed by IDM. Entropy has very poor dynamical ranges for the extreme example simulated above.

In the chapter 4, the four texture parameters are computed above using real radar data.

4. Texture parameter's sensitivity estimates using real radar data

In this chapter the variation of the texture parameters defined in chapter 2 in the case of real weather radar data are investigated by using the data shown in fig. 9 below. This data set is particularly suited for the current investigation as it shows simultaneous presence of both precipitation front approaching from south west (left side of the image) and land and sea clutter regions in the centre and south east regions. Figure 9 is the same data as shown in fig. 1 in chapter 2, except that the current figure shows the pseudo CAPPI product while fig. 1 represent individual elevation scans projected onto the surface.

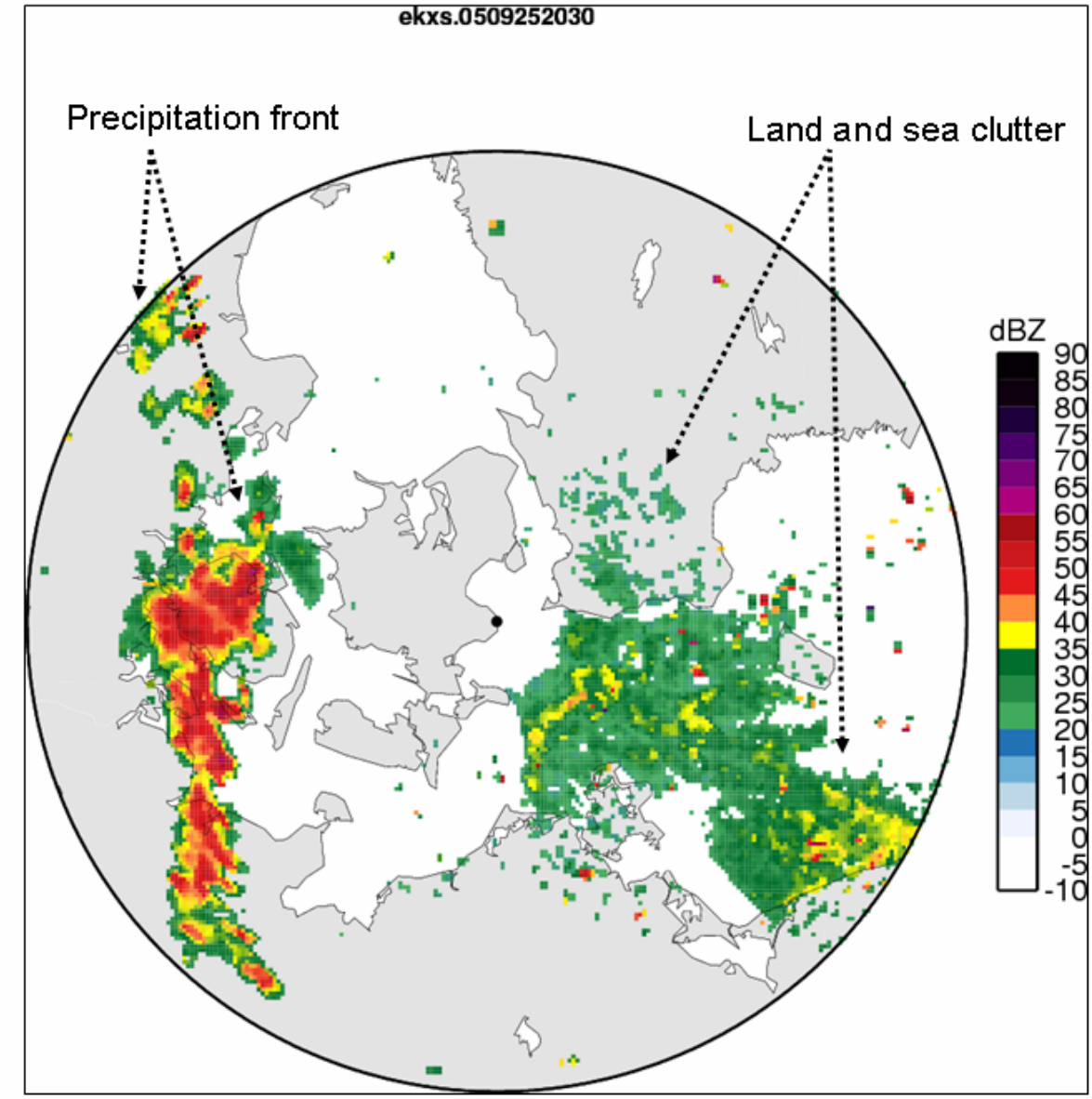

Fig. 9. The pseudo CAPPI product showing the radar reflectivity, Z (dBZ) as measured by the DMI radar situated at Stevns from 25th Sept. 2005 20:30 UTC. The image show a precipitation front on the left and a land and sea clutter from the centre and right of the images. The distance to the outer most circles is 240 km from the centre (position of the radar).

One way to represent the variation of the texture parameters for the different regions of precipitation, land and sea clutter shown in fig. 9 above is to display them on the same colour scale used in the figure above by applying appropriate scaling factors (more details given below).

To determine the sensitivity of the texture parameters to direction, they were computed in the four discrete directions (i) (0° & 180°), (ii) (45° & 225°), (iii) (90° & 270°) and (iv) (135° & 315°). In the results shown below, the following parameter settings were used: $W_A = 1$ (azimuth window size), $(W_R \times W_\phi)$ = (3 X 4) i.e., window consisting of 3 range gates and 4 elevations scan angles with Z_{th} = 0 dBZ and $Z_{\min}$ =10 dBZ. These are the same settings as those used in the last section for the simulated results.

It can be seen from the colour code used to represent the reflectivity values that they lie in the range from -10 dBZ (white tone) to +90 dBZ (black tone). Then to represent the texture parameters using the same colour scale, the parameters inertia, uniformity and IDM were scaled by the factors 90.0/PARmax, where PARmax are the maximum possible values of these parameters, for the above window settings, and are given in table 3 above. For the texture parameter entropy, it was somewhat uncertain as table 3 only gives the minimum values i.e., zero, representing maximum order. To be consistent with the scaling factors used for the other 3 texture parameters, the maximum values of entropy, in the 4 directions were computed directly from the data set in fig. 9. These were 1.45, 5.86, 4.82 and 4.82 in the directions (0° & 180°), (90° & 270°), (45° & 225°) and (135° & 315°), respectively.

4.1 Texture parameters computed in the horizonal directions (0° & 180°)

Figure 10 shows the variation of the texture parameters computed in the horizontal direction. From this figure it can be seen that inertia (top left figure) is zero everywhere (this is shown as transparent in accordance with the display colour map). This follows from its definition and agrees with the simulated results given in the last chapter. Thus from this display it is clear that inertia computed in the horizontal direction will be useless for discriminating between precipitation on one hand and land and sea clutter on the other. In contrast to inertia, uniformity and inverse difference moment appear to be quite efficient at discriminating between precipitation and clutter regions, with perhaps uniformity slightly better than IDM. However, in this case these 2 parameters lie only in the range 0 to 4. Finally, the display of entropy is shown in the bottom right. The dynamical range of entropy values is 0 to 1.45 only, thus the display shows them greatly amplified. However, as entropy is a measure of disorder, it can be seen from this figure that in the precipitation regions, except at the edges, the entropy values are nearly zero (shown as transparent) indicating high degree of order. On the other hand, for the sea and land clutter regions, including at the edges of the precipitation regions on the left, entropy values are relatively higher than those in the precipitation regions which indicate that for these regions there is a much higher degree of disorder.

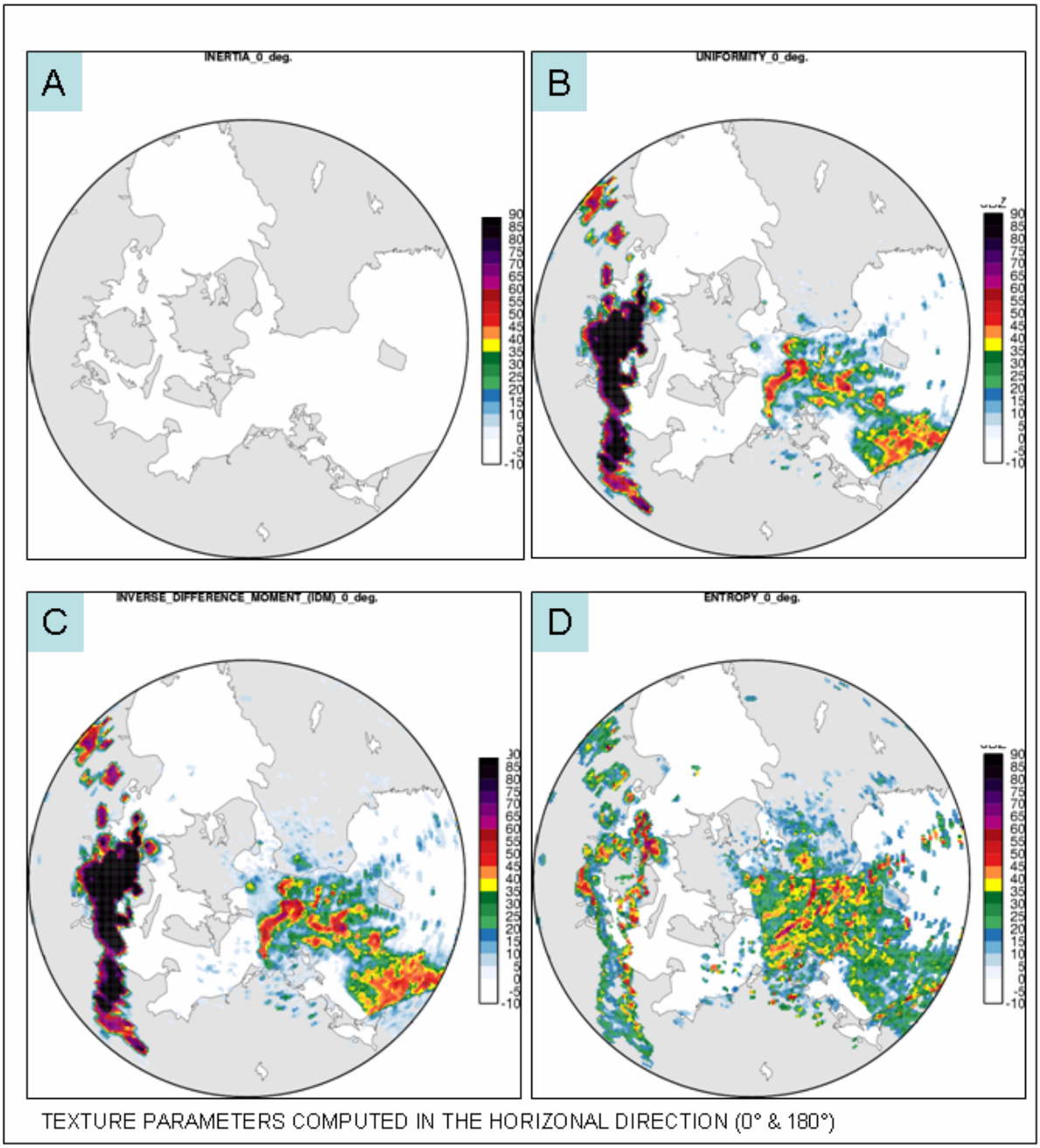

Fig. 10 The values of the four texture parameters INERTIA, UNIFORMITY, INVERSE DIFFERENCE MOMENT and ENTROPY (A, B, C and D respectively), for the radar image shown in fig. 9, computed in the horizontal direction (0° & 180°) shown on a colour scale.

4.2 Texture parameters computed in the vertical directions (90° & 270°)

Figure 11 shows the variation of the texture parameters computed in the vertical direction. From this figure it can be seen that inertia (top left figure) appears to be very good at discriminating between precipitation region on one side and land and sea clutter on the other. However, as can be seen from the figure there are few pixels in the sea clutter regions that have inertia values very similar to their counterparts in the precipitation region, especially at the edges (colour tone green). Similarly, UNIF and IDM appear also to be very good at differentiating between the two categories of signals. However, as can be seen from the figure both of these parameters have relatively higher

values, in the clutter regions, in comparison to the inertia values, and thus they are not as efficient as the latter texture parameter. Further, from table 3, inertia, uniformity and IDM lie in the range: 0 – 40, 0 – 16, 0 – 8, respectively. Thus maximum contrast between the precipitation regions on the one hand and sea and land clutter on the other is expected from the inertia parameter, followed by uniformity and IDM, respectively. Entropy shows also some promise and its values lie in the range 0 – 5.86. In particular, it can be seen that entropy has highest values at the edges of precipitation region and some pixels within the sea clutter area. Further, by comparing these values of uniformity, IDM and entropy with those obtained in the horizontal direction, shown in fig. 10, it can be seen that there is much greater contrast between the values in the sea clutter and the precipitation regions using the vertical direction as opposed to the horizontal.

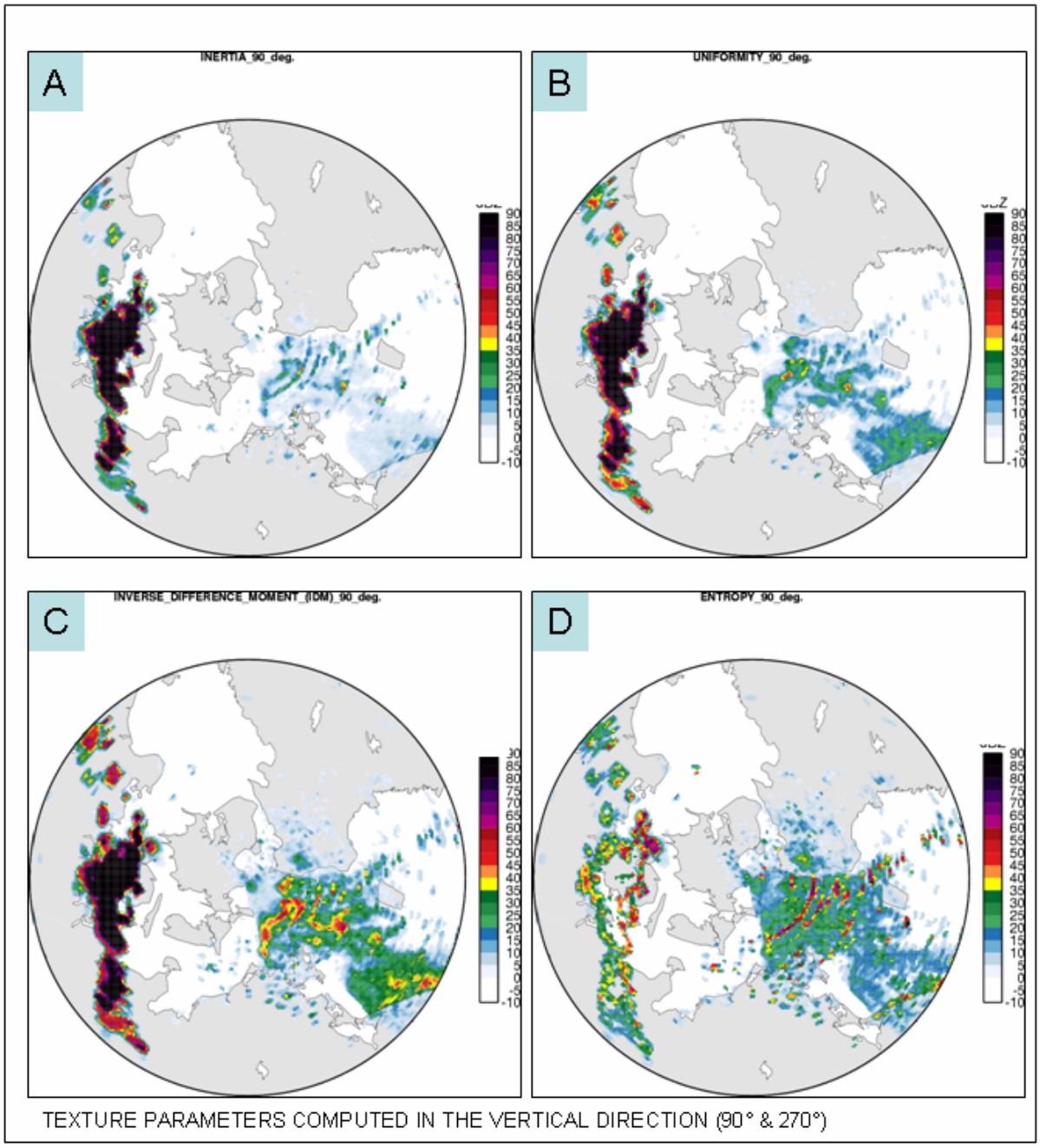

Fig. 11 The values of the four texture parameters INERTIA, UNIFORMITY, INVERSE DIFFERENCE MOMENT and ENTROPY (A, B, C and D respectively), for the radar image shown in fig. 9, computed in the vertical direction (90° & 270°) shown on a colour scale.

4.3 Texture parameters computed in the diagonal directions (45° & 225°)

Figure 12 shows the variation of the texture parameters computed in the diagonal direction (45° & 225°). By comparing these results with those presented in the previous section for the vertical direction (90° & 270°), it can be seen they are very similar. From table 3, inertia, uniformity and IDM lie in the range: 0 – 22, 0 – 14, 0 – 7.8, respectively. A close examination of fig. 12 indicate that perhaps, inertia computed in the vertical case (fig. 11) is slightly better at discriminating between the precipitation and the clutter regions, because there appear to be fewer very high inertia values in the sea clutter region in fig. 11 than in fig. 12. Entropy shows also some promise and its values lie in the range 0 – 4.82 and it appears that, in comparison to fig. 11 above, there are fewer very high entropy values in the current case.

UNIF and IDM do not appear to be significantly different from their values computed in the vertical direction.

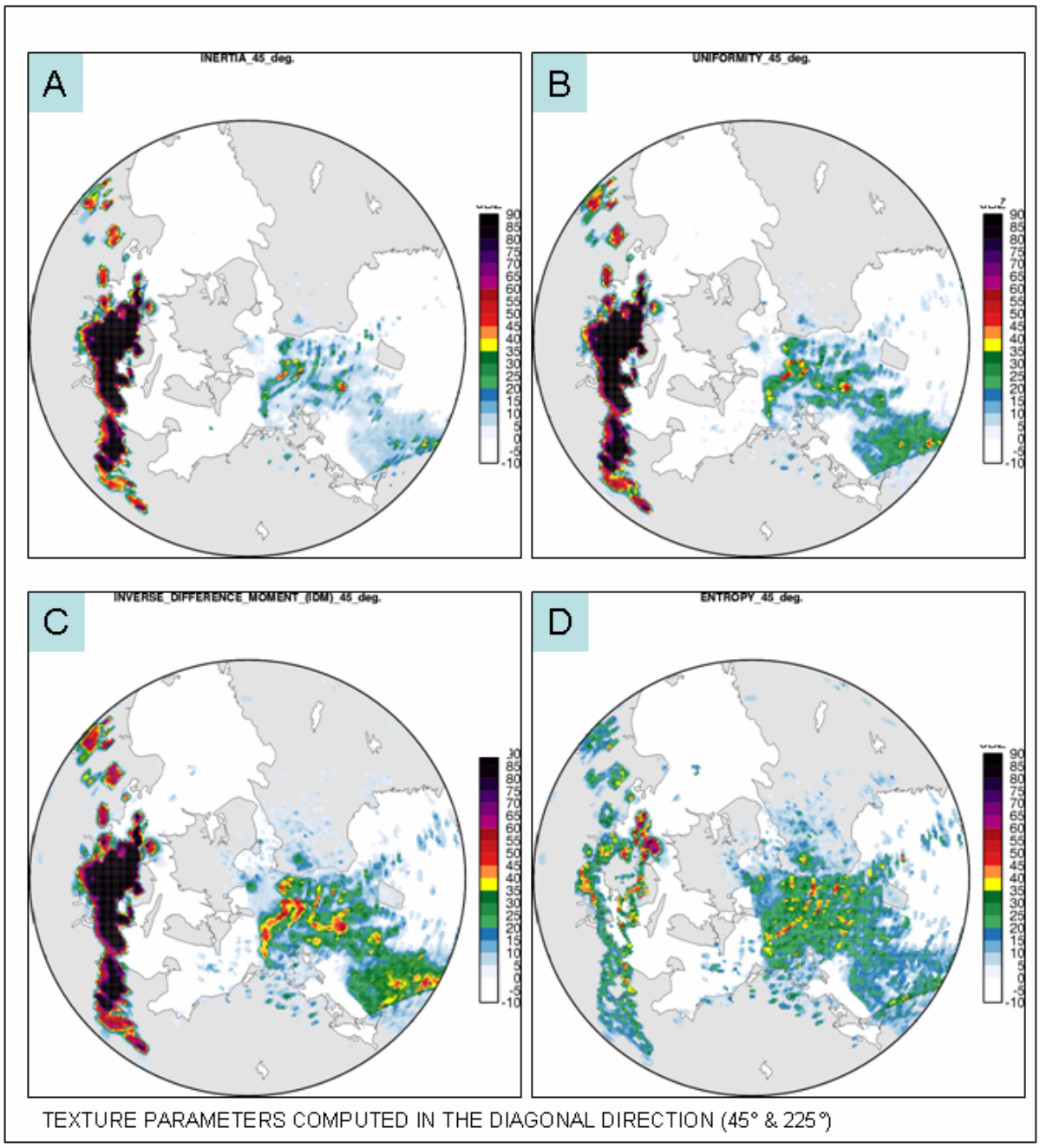

Fig. 12 The values of the four texture parameters INERTIA, UNIFORMITY, INVERSE DIFFERENCE MOMENT and ENTROPY (A, B, C and D respectively), for the radar image shown in fig. 9, computed in the diagonal direction (45° & 225°) shown on a colour scale.

4.4 Texture parameters computed in the diagonal directions (135° & 315°)

Finally, figure 13 shows the variation of the texture parameters computed in the diagonal direction (135° & 315°). By comparing these results with those presented in the previous section for the direction (45° & 225°), it can be seen they are very similar. Also the dynamical range in which the texture parameter lies is identical. From this it can be concluded that computing the texture parameters in the directions (135° & 315°) and (45° & 225°) is not needed as it does not add significant extra information. More specifically, the additional information content in the texture parameters computed in the diagonal directions, in comparison to what is available in the (90° & 270°), is not

significant to justify the extra computations.

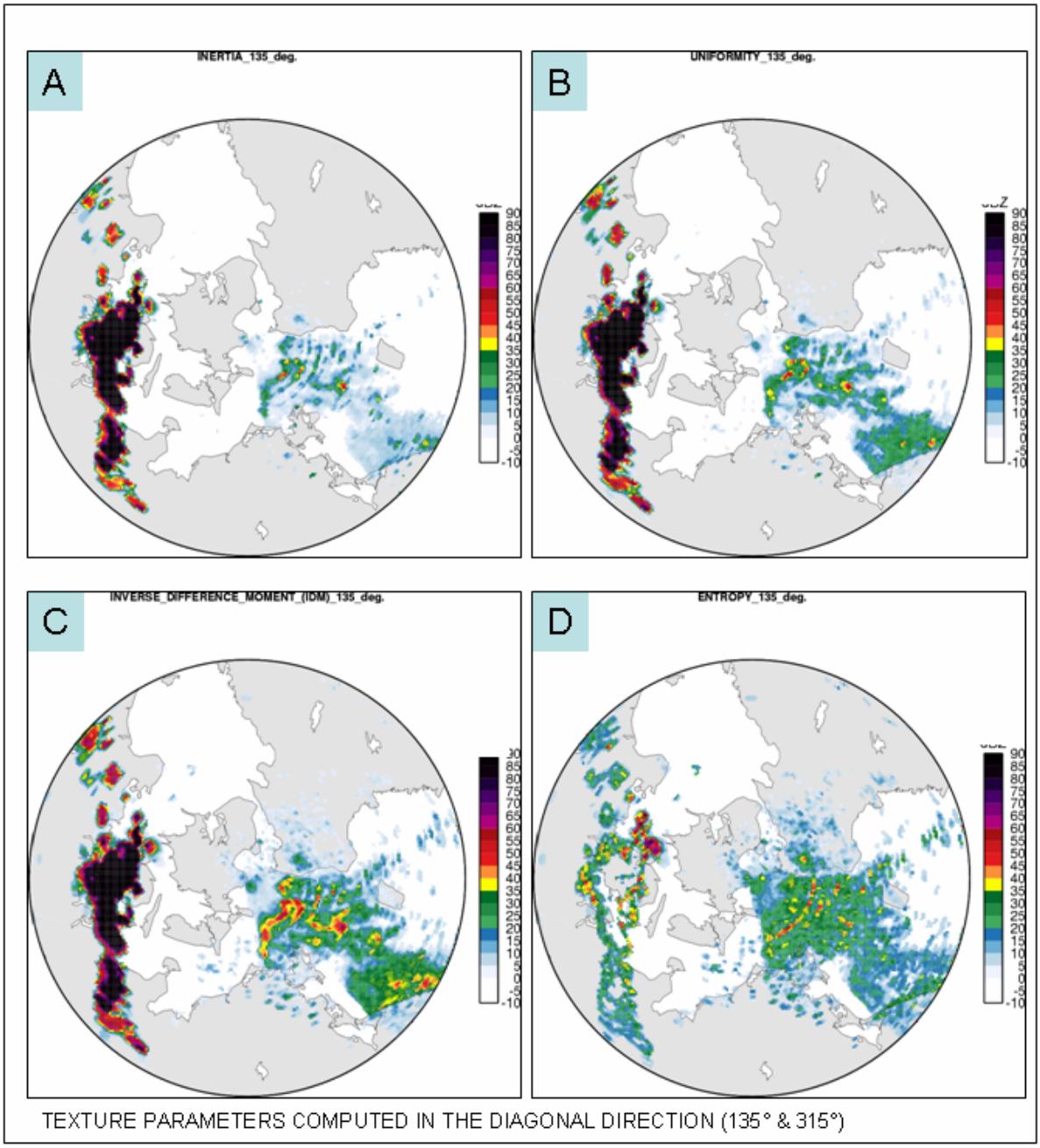

Fig. 13 The values of the four texture parameters INERTIA, UNIFORMITY, INVERSE DIFFERENCE MOMENT and ENTROPY (A, B, C and D respectively), for the radar image shown in fig. 9, computed in the diagonal direction (135° & 315°) shown on a colour scale.

From the results shown in figs. 10 – 13, it can be seen that inertia parameter is the best discriminator between precipitation, on the one hand, and sea and land clutter regions, on the other. This is followed by uniformity, IDM and entropy. Furthermore, as the amount of extra useful information in these parameters computed in the diagonal directions is uncertain, using the inertia parameter computed in the vertical directions (90° & 270°), should provide a useful tool for discriminating between precipitation and clutter regions. This is discussed further in the next chapter.
Finally, in the results presented in above, figs. 10 – 13, the parameter settings were $W_A = 1$ (azimuth window size), $(W_R \times W_\phi)$ = (3 X 4) i.e., a window consisting of one azimuth

angle, three range gates and four elevations scan angles with Z_{th} = 0 dBZ and $Z_{\min}$ = 10 dBZ. The possible dependence of the texture parameters on the values of $W_A, W_R \times W_\phi$, Z_{th} and $Z_{\min}$, were also investigated by repeating the computations for a range of different settings of the above parameters.

4.5 Dependence of the texture measure on different parameter settings

To illustrate the dependence of the texture parameters on the size of the parameters $W_A, W_R \times W_\phi$, Z_{th} and $Z_{\min}$, only the results obtained for different values of the elevation window W_ϕ and minimum values of the reflectivity values, $Z_{\min}$, are worth reporting here. This is because choosing larger values of the windows in the range and azimuth directions only results in smoothing the values of the parameters, and makes the edges less sharp.

Fig.14 shows the displays of inertia computed in the vertical directions for 2 different settings of W_ϕ and $Z_{\min}$. All other parameters were the same as for figs. 10-13. In particular, W_ϕ = 3 i.e., using only the three lowest elevation scan angles (0.5°, 0.7° and 1.0°) and W_ϕ = 4 (0.5°, 0.7° 1.0° and 1.5°) and $Z_{\min}$ = 10 dBZ and 20 dBZ were used. In the top row of fig. 14 $Z_{\min}$ = 10 dBZ and W_ϕ = 4 and 3, (left and right, respectively), while for the bottom row $Z_{\min}$ = 20 dBZ and W_ϕ = 4 and 3, (left and right, respectively). Note that fig. 14A (top left) is same as the fig. 11A above and is shown here for comparison.

From this figure it can be seen that by setting W_ϕ = 3, lot more of the precipitation pixels are now correctly classified, in comparison to the previous case with W_ϕ = 4 (top left). However, this is achieved at the cost of more of the sea clutter pixels having the same grey values as those in the precipitation region. Similarly, increasing $Z_{\min}$ from 10 dBZ to 20 dBZ, in equ. (1), has a positive effect in reducing the inertia values in the clutter region. However, the negative side to this is that lot more of the precipitation pixels, in comparison to the top row, now have the inertia values similar to those in the clutter region. From the results presented in fig. 14 it appears that setting W_ϕ = 3 and $Z_{\min}$ = 20 dBZ, give perhaps the best results. However, since the aim of any clutter removal model is to remove fewer precipitation pixels as possible, a more conservative value of $Z_{\min}$ = 10 dBZ may be more appropriate.

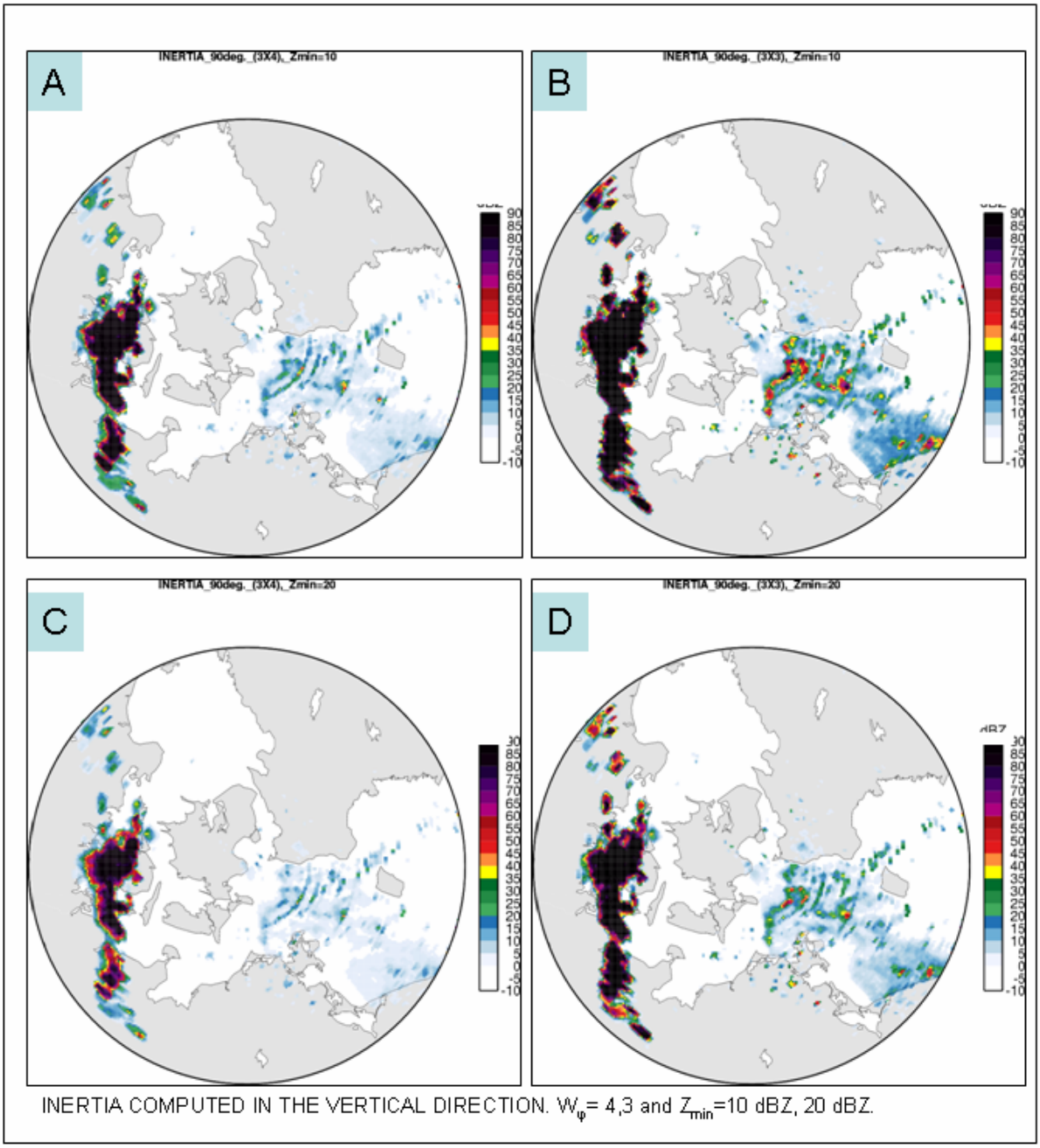

Fig. 14 Colour display of the texture parameter INERTIA computed in the vertical direction (90° & 270°), with $Z_{\min}$ = 10 dBZ and W_{ϕ} = 4 and 3 (top left and right, respectively), and $Z_{\min}$ = 20 dBZ and W_{ϕ} = 4 and 3 (bottom left and right, respectively).

In the next chapter, the results of applying thresholds on the parameter inertia to suppress land and sea clutter are presented.

5. Clutter suppression using second order texture parameter inertia

In the last chapter it was shown that the inertia parameter computed in the vertical directions (90° & 270°), appears to have the best potential at discriminating between the precipitations regions (large values of inertia), on the one hand, and land and sea clutter (low values of inertia) on the other. This texture parameter can now be used to mask regions of land and sea clutter. One approach is to apply thresholds on inertia. In particular, in the first attempt, the following simple criterion is used: if the ratio,

$$\frac{I_{ar}}{I_{\max}} \leq I_{th} \tag{3}$$

then the ground pixel is assumed to contain clutter, else it contain precipitation value. In the above expression I_{ar} represent the value of the inertia parameter for a given azimuth and range gate, and $I_{\max}$ is the maximum possible value of inertia which depends on the number of elevation scans, denoted by W_ϕ, used in the computations. For W_ϕ = 3 and 4, it can be easily shown from (2), that $I_{\max}$ = 12 and 40, respectively. Finally I_{th} is the chosen threshold on the above ratio. In choosing I_{th}, an ideal requirement is that masking of the clutter regions should cause no, or at the most insigificant (from meteoroloigical point of view), disturbance to the precipitation pixels. Alternatively stated, after removing clutter pixels using the above method, some false echoes can still be tolerated but not the removal of precipitation pixels. This is stricter than the criteria sighted in the literature where 'accidental' removal of up to 5% precipitation is tolerated (Wessels and Beekhuis, 1994).

The model proposed above to remove the clutter pixels using the second order inertia parameter depends on the following 6 parameter: W_R, W_A, W_ϕ, Z_{th}, $Z_{\min}$ and I_{th}. From the results presented above the following parameter settings have been used: W_R = 3, W_A =1, Z_{th} = 0 dBZ, W_ϕ = 3 and 4 lowest elevations (= 0.5°, 0.7° 1.0° and 1.5°**)** and $Z_{\min}$ = 10 dBZ and 20 dBZ in equ. (1) for clutter/precipitation discrimination. In the results presented below, the above parameter settings for W_R, W_ϕ, Z_{th} and $Z_{\min}$ were again used, and the most optimal values of the I_{th} were determined by trial and error, by manually comparing the radar images before and after applying the above thresholds on a high resolution computer monitor. These results are presented in figs. 15 – 18 on the following pages. In particular, fig. 15 show the results of attempted removal of land and sea clutter for W_ϕ = 3, $Z_{\min}$ =10 dBZ and 3 different threshold values of I_{th}, namely 0.10, 0.25 and 0.40 (imagettes B, C and D respectively). Also shown in each of the figures 15 – 18, is the original image (imagette A, top left), without any clutter removal, for comparison. In the latter imagette, the two regions of precipitation and land/sea clutter are also identified. The parameters used to compute the results shown in figure 16 are the same as those for fig. 15 above except now $Z_{\min}$ = 20 dBZ. Similarly, the parameter settings used to compute the results shown in figure 17 are the same as those used for fig. 15 except W_ϕ = 4 and I_{th} =0.10, 0.15 and 0.20 (imagettes B, C and D, respectively). Finally, for fig. 18, the parameters used were same as those for fig. 17 except $Z_{\min}$ = 20 dBZ and I_{th} = 0.05, 0.10 and 0.20, (imagettes, B, C, and D, respectively).

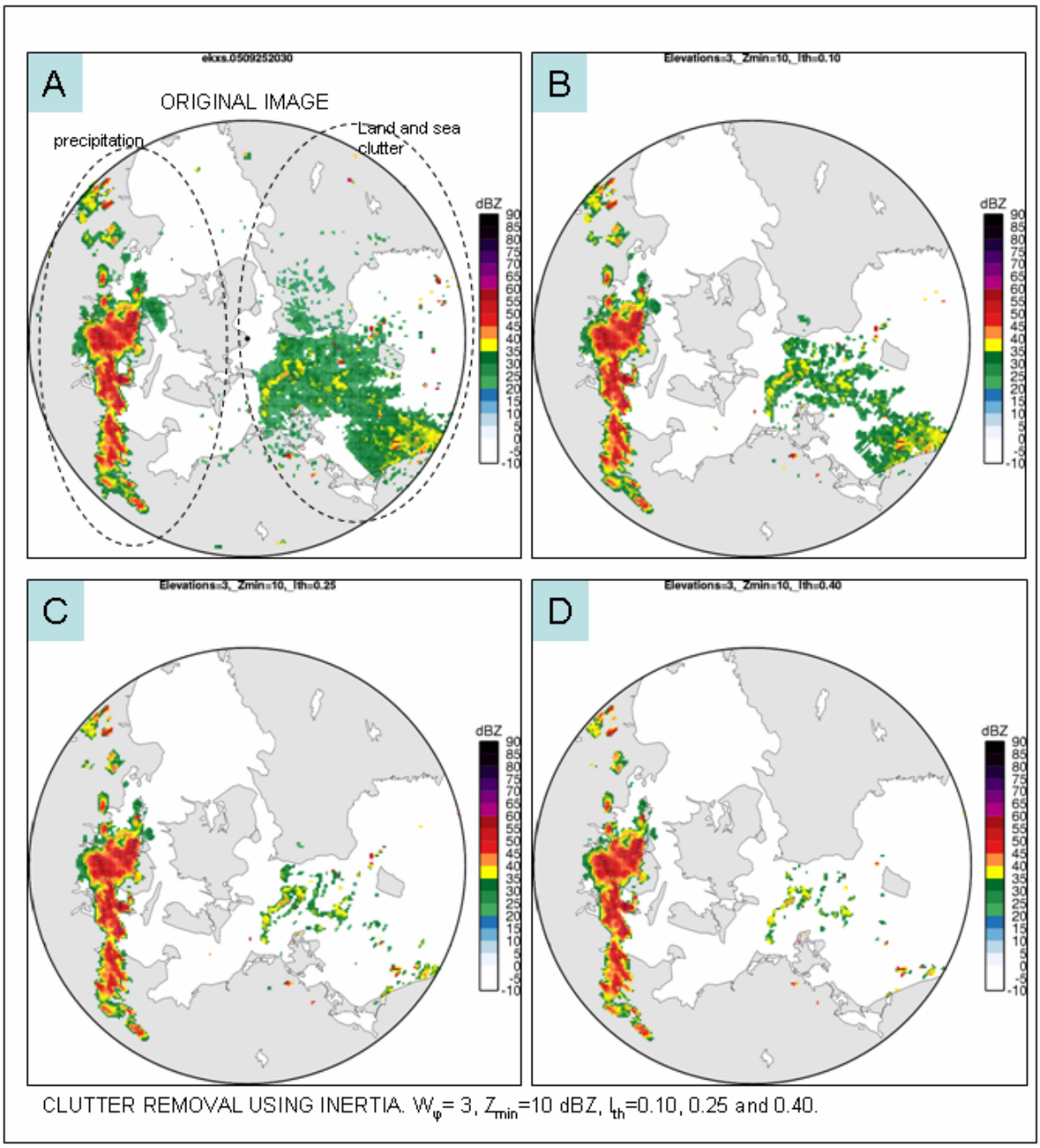

Fig. 15 Clutter removal using the texture parameter INERTIA computed in the vertical direction (90° & 270°), with $Z_{\min}$ = 10 dBZ, W_ϕ = 3 and for 3 different values of the threshold on inertia, I_{th}, 0.10, 0.25 and 0.40 (B, C and D, respectively). Also shown in the figure is the original radar image prior to any clutter removal (top left, A).

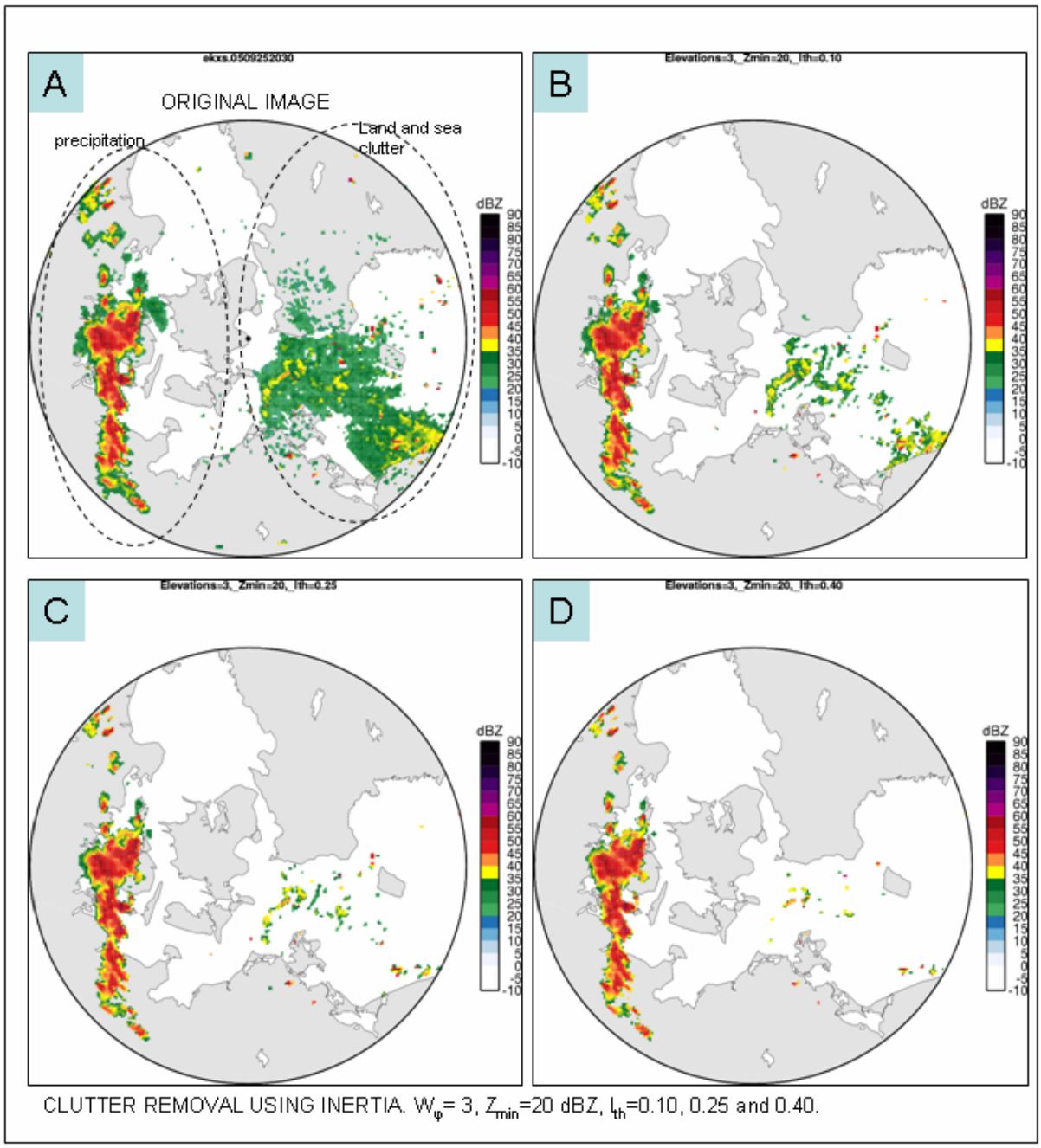

Fig. 16 Clutter removal using the texture parameter INERTIA computed in the vertical direction (90° & 270°), with $Z_{\min}$ = 20 dBZ, W_{ϕ} = 3 and for 3 different values of the threshold on inertia, I_{th}, 0.10, 0.25 and 0.40 (B, C and D, respectively). Also shown in the figure is the radar image prior to any clutter removal (top left, A).

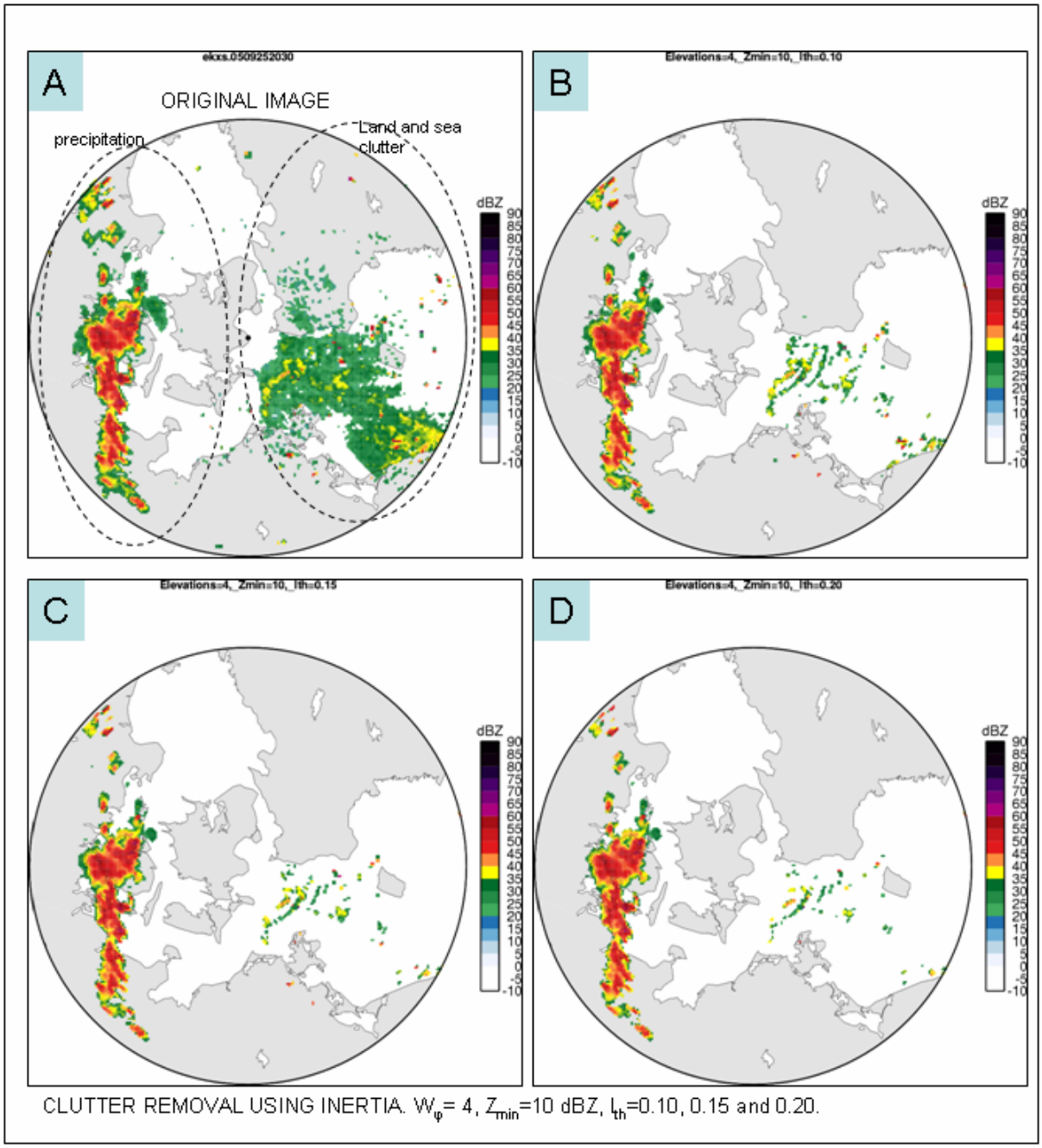

Fig. 17 Clutter removal using the texture parameter INERTIA computed in the vertical direction (90° & 270°), with $Z_{\min}$ = 10 dBZ, W_{ϕ} = 4 and for 3 different values of the threshold on inertia, I_{th}, 0.10, 0.15 and 0.20 (B, C and D, respectively). Also shown in the figure is the radar image prior to any clutter removal (top left, A).

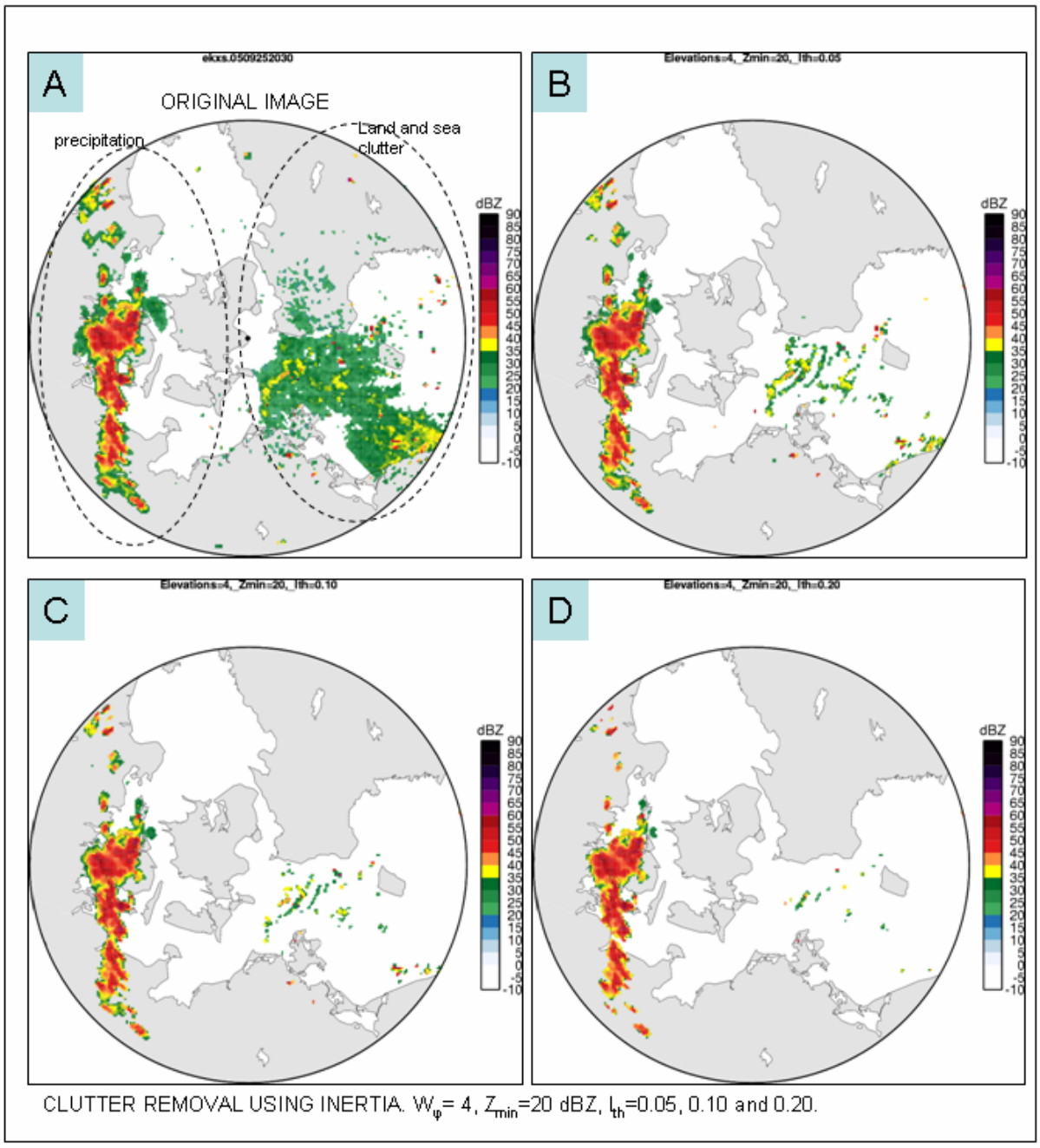

Fig. 18 Clutter removal using the texture parameter INERTIA computed in the vertical direction (90° & 270°), with $Z_{\min}$ = 20 dBZ, W_ϕ = 4 and for 3 different values of the threshold on inertia, I_{th}, 0.05, 0.10 and 0.20 (B, C and D, respectively). Also shown in the figure is the radar image prior to any clutter removal (top left, A).

From the results presented in figs. 15 – 18 above, it can be seen that clutter removal model based on the inertia parameter is quite efficient. However, it is also apparent form the above results that the technique has the unwanted effect of removing some precipitation pixels. The latter is dependent on the values of the parameters: W_R, W_A, W_ϕ, Z_{th}, $Z_{\min}$ and I_{th} used to run the algorithm. Similar results are also obtained using other radar data sets. From this one can conclude that, despite the fact that the elevation angles dependent texture parameters proposed above are effective at discriminating between precipitation and land/sea clutter regions in most of the regions, there are some pixels for which the texture parameters have very similar values. The latter is especially true in case of low lying, weak precipitation regions (≤15 dBZ – 20 dBZ) which then are also 'accidentally'

removed.

The above results are not surprising. Similar conclusions have been reached previously, namely, that attempts at removing clutter, at least in single polarisation weather radar data, results in some loss of precipitation pixels (Wessels and Beekhuis, 1994, Alberoni et. al., 2001, Steiner and Smith, 2002, Kissinger, 2003). Some conditions are usually proposed for the model to be declared useful, such as the minimum percentage of clutter pixels acceptable and/or the maximum percentage of precipitation pixels 'accidentally' removed after the clutter removal model been applied to the radar data. However, it is felt that although certain percentage of clutter pixels may be tolerated after attempted removal, the fact that some precipitation also gets removed is difficult to accept. For this reason, a general application of the clutter removal algorithm for entire region covered by the radar is not recommended. Instead, it is proposed to apply the above model at specific regions of land/sea clutter 'hot spots' where the latter is frequently observed. In this way one can minimize the 'accidental' removal of precipitation pixels.

In the chapter 6, one such model is proposed. It concerns the removal of sea clutter from DMI's weather radar at Stevns on Sjælland.

6. Sea clutter removal model for the DMI's radar at Stevns

Based on the conclusion reached in the last chapter, it has been recommended not to apply the model developed above to remove both land and sea clutter over the entire area monitored by the weather radars as the expected 'accidental' removal of precipitation pixels is unacceptable. To minimize the risk of removing precipitation pixels, it was thus recommended to instead concentrate on the sub-regions, the so-called 'hot spots', where anaprop is frequently observed and also to make use of any additional relevant, radar specific, information, such the possible seasonal dependence of the sea clutter at the radar. The usefulness of this model is illustrated by applying it to remove the sea clutter that is frequently observed by the DMI's weather radar situated on the main island of Sjælland at Stevns; about 50 meters from the Baltic Sea coast (55.326°N, 12.449°E).

The main components of the algorithm are outlined next.

6.1 Components of the sea clutter removal algorithm

The model consists of 2 main components:

1. A sea mask identifying the regions where the sea clutter is frequently observed.
2. Pre-processing or identifying the criteria that can be used to determine when sea clutter is likely to take place so that sea clutter algorithm can be applied. The latter also include any other relevant information that is specific to the radar such as the observed seasonal dependence of sea clutter.

The DMI's radar at Stevns has been in operations since 2002. Based on the analysis of the data since then it has been concluded that the main regions where sea clutter is observed is shown in fig. 19. In particular, in the figure two shaded of blue have been chosen to indicate the potential anaprop "hot spots", the darker of which designate the region where sea clutter is observed more frequently than the other.

Fig. 19 Sea clutter mask used to designate the regions (shaded in blue) where sea clutter is frequently observed at Stevns. The dark blue region is where sea clutter is observed more frequently than the areas shown in lighter blue.

Thus the sea clutter removal model will only be applied to the regions shaded in blue in fig. 19. All other regions monitored by the radar are left completely unchanged.

As regards pre-processing the following simple criteria have been used so far:

1. For the time being, sea clutter season is assumed to take place over a fixed period e.g., from 25th March – 15th October. Thus only during this period is any action taken to remove sea clutter in the radar data.

2. During the anaprop season, the following criteria are used to determine whether to execute the algorithm:

    a. If the number of pixels in the dark blue region in fig. 19 are greater than in the rest of area monitored by the radar, and if more than 50% of the pixels in the dark blue region have normalised inertia less than I_{th_0}, then anaprop is assumed to be present in the dark blue region and the sea clutter algorithm is applied.
    b. Alternatively, if the percentage of the inertia pixels in the dark blue region are less than I_{th_1}, with $I_{th\_1} >> I_{th\_0}$ then AP is again assumed to be present in this sector and the algorithm is executed to remove it.

c. If the either of the above 2 criteria are true, and in addition if percentage of the inertia pixels in the lighter blue regions of fig. 19 are less than I_{th_2}, with $I_{th\_2} << I_{th\_1}$ then AP is also assumed to be present in the lighter blue regions and attempt is made to remove it.

One of the negative consequences of applying the above pre-processing criteria is that weak low lying precipitation front may still be misclassified as sea clutter and thus may be 'accidentally' removed.

In future, the information content of high resolution numerical weather prediction models and the relevant satellite data will be investigated to determine how far they can assist in flagging when and where to apply the anaprop removal algorithm. It is hoped that the information in these external sources has sufficient spatial and temporal resolution so that the need to use citerion 1 above and the sea clutter mask of fig. 19 can be relaxed.

6.2 Test results

The result of applying the above simple pre-processing criteria and the sea mask can be seen in fig. 20. In this figure, the image on the left is the original radar image, while that on the right is after applying the sea clutter removal algorithm.

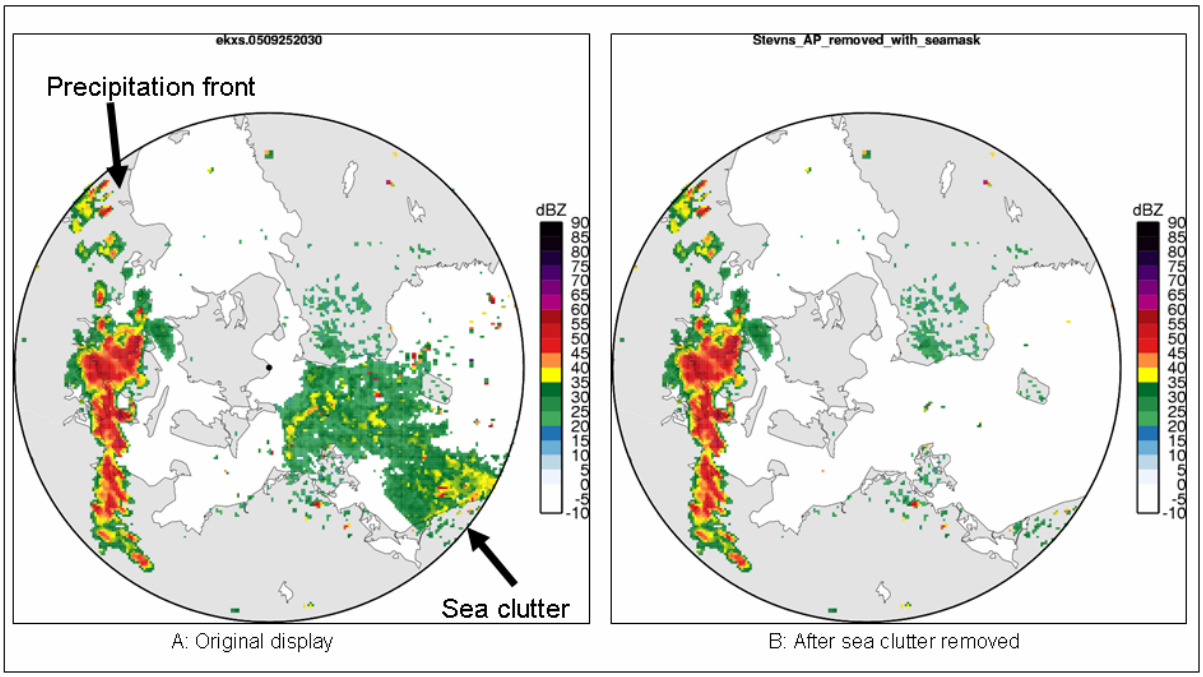

Fig. 20 Removal of the sea clutter observed at DMI's radar at Stevns using the sea mask shown in fig. 19. Original display is shown on the left for comparison.

As can be seen from fig. 20 after applying the sea clutter removal model, few false echo pixels in the area of concern are still present. This is due to the current settings of the 3 parameters: W_ϕ, $Z_{\min}$ and I_{th} which have been deliberately kept somewhat conservative so as to reduce the likelihood of the model removing real precipitation pixels in case the pre-processing steps listed above misclassify a possible, low lying, weak precipitation in the region (≤ 15 dBZ – 20 dBZ) as sea clutter. Note that, because of the region chosen where to apply the algorithm, land clutter has not

been removed.

The above pre-processing steps and the thresholds on the parameters have since been tested and fine tuned by applying them on an extensive data sets that are known to be contaminated with sea clutter. The evaluation of the model during routine operations is now in progress.

In the chapter 7 the main results and conclusions reached so far are summarised.

7. Summary

One of the most serious problems with using weather radar to detect and measure precipitation is the presence of false echoes, especially the so-called land and sea clutter. Ever since weather radars were first used to monitor the atmosphere, attempts have been made to separate and remove these false echoes from the data. Of these false echoes, those that occur over the sea are perhaps the most difficult to eliminate as the radar returns from the sea can be of comparable strength (~ 15 dBZ - 20 dBZ is not uncommon), and have similar doppler velocities, to radar returns from precipitation regions. The studies that have been reported in the literature to address this problem can be split into three categories; (i) advanced data classification schemes such as those based on fuzzy logics or neural networks using parameters derived from the radar moments corrected reflectivity (Z), doppler velocity (V) and occasionally the doppler spectral width (W) (Lakshmanan et. al., 2003, Kissinger et. al., 2003), (ii) methods based predominately on thresholds applied on Z, gradients of Z, and/or differences of Z at different altitudes or elevation angles (Steiner and Smith, 2002, Albernoi et. al., 2001), and finally (iii) making use of data and products derived from other sensors such as satellites or numerical prediction models to identify and eliminate false echoes (Lakshmanan and Valente, 2004, , Bøvith et. al., 2006). Further, new types of parameters have also been proposed such as SPIN, SIGN and FUP, the Frequency of Unbroken Profiles to remove clutter in (i) and (ii) above (Steiner and Smith, 2002, Kissinger et. al., 2003, Albernoi et. al., 2001).

In many of the threshold methods outlined above, attempts are made to make use of information related to the vertical profile of reflectivity, Z; e.g., gradients of Z and/or differences of Z at different elevation scans, or parameter such as FUP measuring the frequency of vertical unbroken profiles. The reason why reflectivity values at different elevation scans are so important for anaprop recognition is that it has long been observed that clutter signals have little vertical extent and that they tend to be confined to low elevation angles, typically ≤1.5°- 2.0º. Thus one way to improve anaprop recognition in weather radar data is to devise more effective altitude dependent texture parameters. One such method is proposed and is the subject of this report. In particular, a new matrix by analogy with the GCLM is proposed. However, unlike the GLCM which is a measure of the number of occurrences of two neighbouring pixels, at two different locations with grey values i and j, the current matrix is a measure of the number of occurrences of pixels at elevation angles I and J having reflectivity values > $Z_{\min}$. The matrix is computed over a 3 dimensional window of size ($W_R \times W_A \times W_\phi$) where W_R, W_A and W_ϕ are its dimension in the radial, azimuth and elevation direction (= number of elevation scans), respectively. One of the striking features of the current model is that the contribution made by low to modest reflectivity values, Z ≤ $Z_{\min}$, is also included. Currently the latter is modelled using a simple linear relationship (equ. (1)).

By analogy with the GLCM a number of texture parameters can be defined and these are used to determine their effectiveness at distinguishing between sea clutter and precipitation. In the evaluation carried out so far the texture parameters entropy, inertia, uniformity and inverse difference moment (IDM) have been used. It was found that the parameter inertia was exceptionally effective at discriminating between the sea clutter and precipitation. This result was then used to remove the clutter regions in the radar data by applying thresholds on the inertia parameter. The results showed that when this is applied in general to the whole of the radar data, it was found that, in addition to the removing clutter pixels, it also results in the removal of some precipitation pixels. The actual number of precipitation pixels removed is dependent on the model parameters such as threshold on inertia and the values of W_R, W_A, W_ϕ and $Z_{\min}$. This result is in agreement with previous findings, namely that a perfect land and sea clutter removal model for the single polarisation mode radars, is difficult. However, as the ‘accidental’ removal of any precipitation is unacceptable to the user community, a modest application of the clutter removal is proposed. In

particular, to minimize the 'accidental' removal of precipitation pixels, it is proposed to implement a land and/or sea clutter removal algorithm for the individual radars, making use of the additional information that is specific to the radar. The latter can, for example, be restricting the application of the clutter removal model to specific geographical 'hot spots' where clutter is frequently observed by the radar and taking into account other relevant local information such as its seasonal dependence. One such model, to remove the sea clutter, has been developed for the Danish Meteorological Institute's (DMI) radar at Stevns on the island Sjælland (55.326°N, 12.449°E). The evaluation of the model undertaken so far looks encouraging. Further tests of the model, during routine operations, are in progress.

As discussed above, one of the main draw back with the current and previous algorithms is that none of them is perfect. In particular, when using the above algorithms to remove false echoes, it always results in the 'accidental' removal of real precipitation pixels. Because of this reason developing operationally more robust clutter removal algorithms is an ongoing activity.

The areas where further improvement in the model is possible are:

1. So far to include the contribution to texture by reflectivity values $Z \leq Z_{\min}$ a simple linear relationship has been used (eq. (1)). Other, more complex relationships, such as reflectivity gradients, can be used.
2. The elements of the EDCM matrix, denoted by N_{ij}, are not computed in the true 3 dimensional, as in the current model they are defined as the number of occurrences of radar gates, *for a fixed single value of azimuth angle,* A_k, at locations (R_1, ϕ_i) and (R_2, ϕ_j), having a pair of reflectivity values $> Z_{\min}$. Thus the 3rd dimension, azimuth, is only partly included. Possible improvement could be to extend this definition at locations (R_1, A_1, ϕ_i) and (R_2, A_2, ϕ_j). Further the diagonal elements of N_{ij} are *not pair of values*, rather just single reflectivity values. Although, the individual reflectivity values of the elevation gates are important for clutter/precipitation discrimination, however, a more consistent definition is required. Note that for inertia, diagonal elements of N_{ij} play no part as they are all zero.

Finally, as been concluded by previous studies, there is a limit to how much net useful information one could extract out of the radar reflectivity data to discriminate between clutter/precipitation. In some cases, especially low lying weak precipitation regions, the reflectivity values and their vertical profiles are indistinguishable from their counterpart in the clutter areas, at least using statistical analysis. Thus a more rewarding approach could be not to base the classification on the radar reflectivity values alone, but rather combine with other moments (e.g., for single polarisation radars V and W) and make use of data/products from other sensors such as satellites, rain gauges, numerical weather prediction models.

8. Acknowledgement

The author wish to thank Thomas Bøvith with the development of the radar display software and Georg B. Larsen for editing the text.

9. References

Alberoni P. P., Andersson T., Mezzasalma P., Michelson D. B., and S. Nanni.: "Use of the vertical Reflectivity profile for Identification of Anomalous propagation", Meteorol. Appl. 8, pp. 257 – 266., 2001.

Batten, L. J.:"Radar Observations of the Atmosphere", University of Chicago Press, Chicago, 1973.

Booker, H. G.: "Elements o Radio Meteorology: How Weather and Climate Cause Unorthodox Radar Vision beyond the Geometrical Horizon, J. IEE, vol. 93, pt.IIIA, pp.69 – 78, 1946.

Bringi V. N. and V. Chandrasekar: "Polarimetric Doppler Weather Radar: Principle and Applications", Cambridge press. 2001.

Bøvith T., Gill R. S., Overgaard S. Hansen L. K. and A. A. Nielsen, "Detecting Weather radar Clutter Using Satellite Based Nowcasting Products", Proc. of 4th European Conf. on Radar in Meteorology and Hydrology, 2006.

Doviak, R. J. and D. S. Zrnic: " Dopller Radar and Weather Observations", Academic Press, Second Edition, 1993.

Gill R. S.: "Operational Detection of Sea Ice Edges and Icebergs using SAR", Canadian J. Remote Sensing, vol. 27, No. 5, 2001.

Haddad B., Adane A., Sauvageot H., Sadouki L., and R. Naili.: "Identification and Filtering of Rainfall and ground radar Echoes using Texture Features", Int. J. Remote Sensing, vol. 25, No. 21, pp. 4641 – 4656, 2004

Kessinger C., Ellis S., and J. Van Andel.: "The Radar Echo Classifier: A Fuzzy Logic Algorithm for the WSR-88D", 19th IIPS Conf., Amer. Meteo. Soc. Long Beach, CA., 2003.

Lakshmanan V. and Valente M.: "Real-Time Quality Control of reflectivity data Using Satellite Infrared Channel and Surface Observations", 20th Int'l Conf. on Inter. Inf. Proc. Sys. (IIPS) for Meteor. Ocean. And Hydro., Amer. Met. Soc. Seattle, 2004.

Lakshmanan V. Hondl K., Stumpf G. and T. Smith: "Quality Control of weather Radar data using Texture Features and a Neural Network", 5th Int'l Conf. on Adv. In Pattern Recog., IEEE, Kotkota, 2003.

Michelson D. B. and Sunhede, D: "Spurious Weather Radar Echo Identification and Removal using Multisource Temperature Information, Meteorological Applications, 11, pp. 1-14, 2004.

Meischner P. (Ed.): "Weather Radar", Springer – Verlag Berlin Heidelberg, 2004.

Ryzhkov A., "The Effect of Nonuniform Beam Filling on the Quality of Radar Polarimetric Data", Proc. of 4th European Conf. on Radar in Meteorology and Hydrology, 2006.

Shokr M. E.: "Evaluation of Second-Order Texture Parameters for Sea Ice Classification From Radar Images", J. Geo. Res. Vol. 96, No. C6, pp. 10625 – 10640. 1991.

Skolnik M. I.: "Introduction to Radar Systems", McGraw-Hill International Editions, Second edition, 1981.

Steiner, M. and J. Smith.: "Use of Three Dimensional Reflectivity Structure for Automated Detection and Removal of Non-Precipitation Echoes in Radar Data", J. Atmos. Ocea. Tech. pp. 673 – 686, 2002.

Sugier J. and P. Tabary. "Evaluation of Dual Polarisation Technology at C-band for Operational Weather radars as part of the EUMETNET OPERA program", Proc. of 4th European Conf. on Radar in Meteorology and Hydrology, 2006.

Wessels H. R. A. and J. H. Beekhuis: "Stepwise Procedure for Suppresion of Anomlaoug Ground Clutter, COST-75 Seminar on Advanced radar Systems, EUR 16013 EN, pp. 270 – 277, 1994.

Previous reports

Previous reports from the Danish Meteorological Institute can be found on:
http://www.dmi.dk/dmi/dmi-publikationer.htm